

# A control-oriented approach to optimal sensor placement\*

Madhusudan Madhavan<sup>†</sup>, Alen Alexanderian<sup>‡</sup>, Arvind K. Saibaba<sup>§</sup>, Bart van Bloemen Waanders<sup>¶</sup>, and Rebekah D. White<sup>||</sup>

**Abstract.** We propose a control-oriented optimal experimental design (cOED) approach for linear PDE-constrained Bayesian inverse problems. In particular, we consider optimal control problems with uncertain parameters that need to be estimated by solving an inverse problem, which in turn requires measurement data. We consider the case where data is collected at a set of sensors. While classical Bayesian OED techniques provide experimental designs (sensor placements) that minimize the posterior uncertainty in the inversion parameter, these designs are not tailored to the demands of the optimal control problem. In the present control-oriented setting, we prioritize the designs that minimize the uncertainty in the state variable being controlled or the control objective. We propose a mathematical framework for uncertainty quantification and cOED for parameterized PDE-constrained optimal control problems with linear dependence to the control variable and the inversion parameter. We also present scalable computational methods for computing control-oriented sensor placements and for quantifying the uncertainty in the control objective. Additionally, we present illustrative numerical results in the context of a model problem motivated by heat transfer applications.

**Key words.** optimal control, inverse problems, Bayesian inference, optimal experimental design, sensor placement.

**AMS subject classifications.** 65M32, 49N45, 62K05, 62F15, 35R30, 65C60.

**1. Introduction.** Optimal control of systems governed by partial differential equations (PDEs) is a commonly occurring problem in the sciences and engineering. Examples of control problems can be found in wildfires, sub-surface petroleum reservoirs, HVAC systems, experimental fusion energy, and additive manufacturing [27, 35, 39, 59]. A key challenge in such optimal control problems is the presence of uncertain parameters in the governing PDEs. Examples of such parameters include coefficient functions, volume of boundary source terms, or initial conditions.

---

\***Funding:** Madhavan was supported by the National Science Foundation through the award DMS-1745654. Saibaba was supported, in part, by the Department of Energy through the award DE-SC0023188. The work of Alexanderian and van Bloemen Waanders was supported in part by the U.S. Department of Energy, Office of Science, Office of Advanced Scientific Computing Research Field Work Proposal Number 23-02526. Madhavan and Saibaba were also supported, in part, by the National Science Foundation through the award DMS-2411198.

<sup>†</sup>Department of Mathematics, North Carolina State University, Raleigh, NC, USA,

<sup>‡</sup>Department of Mathematics, North Carolina State University, Raleigh, NC, USA,

<sup>§</sup>Department of Mathematics, North Carolina State University, Raleigh, NC, USA,

<sup>¶</sup>Sandia National Laboratories,

<sup>||</sup>Sandia National Laboratories

Consider, for example, a control problem of the form

$$\min_z \Phi_{\text{ctrl}}(u(z), z; m)$$

where

$$(1.1) \quad \begin{cases} \frac{\partial u}{\partial t} = \mathcal{G}(u, z, m), \\ u(\cdot, 0) = u_0. \end{cases}$$

Here,  $u$  is a state variable,  $z$  is a control,  $m$  is an uncertain parameter, and  $\Phi_{\text{ctrl}}$  is a suitably defined reduced cost functional. In the present work, we consider the case where the goal of the control problem is to steer the state variable toward a desired target terminal state. Note that the resulting optimal control problem is parameterized by the uncertain parameter  $m$ .

A key challenge in such parameterized optimal control problems is that the computed optimal control might depend strongly on the value of the uncertain parameter  $m$ . Therefore, having access to a reliable estimate of  $m$  is important. Often, we can estimate  $m$  by solving an inverse problem. In the present work, we consider a Bayesian paradigm [55, 56], in which we use a model and data to find a posterior distribution law for  $m$ . Not only does this provide a useful point estimate for  $m$ , given by the maximum a posteriori probability (MAP) point, it also enables quantifying the uncertainty in the optimal control or the control objectives. In a nutshell, to enable solving the optimal control problem with quantified uncertainties, we need to perform the following steps:

- (i) acquire measurement data;
- (ii) solve an inverse problem to estimate  $m$ ; and
- (iii) solve the optimal control problem.

Note, however, that step (i) often involves a costly process. Namely, acquiring experimental data can be time-consuming and is subject to physical and/or budgetary constraints. Thus, it is crucial to collect data optimally. This requires solving an optimal experimental design (OED) problem [8, 51, 60]. In the present work, we consider a Bayesian approach to OED [17].

Traditional approaches to Bayesian OED provide techniques for minimizing uncertainty in the inversion parameter  $m$ . However, these approaches are not well-suited for problems in which the estimation of the inversion parameter is merely an intermediate step. Specifically, finding a data acquisition strategy that is tailored to parameterized optimal control problems requires a *control-oriented OED (cOED)* framework. This is the primary focus of this article. In particular, cOED involves coupling three different problems: (i) an optimal control problem; (ii) an inverse problem; and (iii) an optimal sensor placement problem. A schematic indicating the different components of such a framework is depicted in Figure 1.

In the present work, we take a foundational step in developing a mathematical and computational framework for inversion, design of experiments, and control for systems governed by PDEs with infinite-dimensional uncertain parameters. We consider the case where  $\mathcal{G}$  in (1.1) is linear in  $u$ ,  $z$ , and  $m$ . This setup covers problems involving the control of systems governed by linear PDEs where (i) we seek controls in boundary or volume source terms; and (ii) have uncertainties in the remaining source terms in the governing equations. We focus on problems in which the inversion parameter  $m$  is estimated using measurement data collected at a set of sensors. Moreover, we assume a linear (or linearized) model governing the inverse

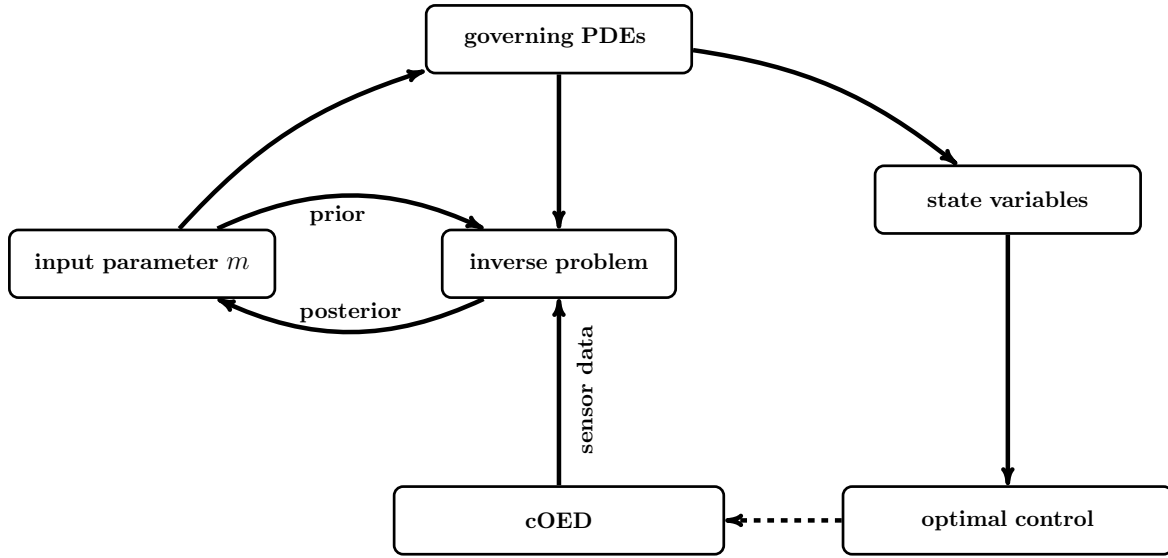


Figure 1: The various aspects of optimal control, inversion, and design of experiments. The optimal control problem informs the definition of a cOED criterion. Subsequently, we solve the cOED problem (to obtain sensor data), the inverse problem (to estimate  $m$ ), and the optimal control problem. In the diagram, the governing PDEs include the PDEs governing the inverse problem and those governing the control problem.

problem. To elucidate the components of the coupled optimal control, inversion, and cOED formulations, we present a motivating model problem formulation, involving a heat transfer application, in [Section 2](#). The requisite background regarding inversion, design of experiments, and optimal control in the class of problems under study is outlined in [see Section 3](#).

**Related work.** Design of experiments for large-scale Bayesian inverse problems has been subject to intense research activity in recent years; see the review articles [\[2, 36\]](#) for a survey of the literature. Optimal control of systems governed by PDEs under uncertainty has also been investigated in various studies; see, e.g., [\[5, 13, 18, 28, 41, 58\]](#). The present work takes a foundational step in bridging the gap between optimal design of experiments for inverse problems governed by PDEs and optimal control under uncertainty. The proposed approach is related to recent efforts on *goal-oriented* OED [\[15, 33, 44, 62\]](#). Namely, cOED can be considered as a type of goal-oriented OED, with a specific goal that is informed by an optimal control problem. The developments in the present work are related to the works [\[9, 61\]](#), which consider goal-oriented optimal design of infinite-dimensional linear Bayesian inverse problems. While there has been some efforts on relating optimal control to the design of experiments [\[23, 34, 50\]](#), to our knowledge, there have been no efforts on a control-oriented approach to the optimal design of experiments for Bayesian inverse problems.

**Our approach and contributions.** We consider the average variance in the terminal state,  $u(\cdot, T_{\text{final}})$ , as our choice of design criterion. We call this the *cOED criterion*. This criterion takes the form of a weighted A-optimality criterion that combines constructs in the

inverse and optimal control problems. Upon finding an optimal sensor placement, we can solve the inverse problem to estimate  $m$ . Subsequently, the optimal control problem is solved with  $m$  taken as the MAP point. However, the terminal state and the optimal control objective are still uncertain, due to the uncertainty in  $m$ . To address this, we also develop a mathematical framework for quantifying the uncertainty in the optimal control objective. This includes expressions for mean and variance of the control objective as well as a concentration bound. The latter provides important qualitative insight regarding the importance of optimizing our cOED criterion. Namely, we show that the cOED criterion can be used to bound the probability of large deviations in the control objective. The proposed framework for quantifying the uncertainty in the terminal state and the optimal control objective is detailed in [Section 4](#).

The expressions for the cOED criterion and measures of uncertainty in the optimal control objective involve traces of high-dimensional operators that are defined only implicitly. To enable implementations in large-scale applications, we provide fast and accurate computational methods for the various steps of the proposed control-oriented optimal experimental design and uncertainty quantification framework. These include fast methods for computing the cOED objective and the mean and variance of the control objective. The proposed approach builds on randomized trace estimators and structure-exploiting approaches for Bayesian inversion in a function space. The proposed computational framework for cOED and uncertainty quantification for parameterized optimal control problems is presented in [Section 5](#).

The key contributions of this article are

- An end-to-end mathematical framework for uncertainty quantification and cOED for parameterized PDE-constrained optimal control problems with linear dependence to the control variable and the inversion parameter;
- computational methods for fast evaluation of the cOED objective as well as measures of uncertainty in optimal state trajectory and optimal control objective; and
- concentration bounds for the control objective, relating the proposed cOED objective to the deviations in the control objective.

Additionally, we elaborate the proposed framework for cOED in [Section 6](#), in the context of the heat transfer problem discussed in [Section 2](#). Our extensive numerical results demonstrate the effectiveness of the proposed strategy. In [Section 7](#), we present concluding remarks and discuss the limitations of the present study and potential directions for future work.

**2. Motivating application and model problem.** In this section, we consider a model problem to illustrate the types of interconnections between optimal control, parameter inversion, and optimal experimental design (OED) that might arise in applications. The following example builds on well-known example found in inverse problem literature [[1](#), [22](#), [40](#), [49](#)], as well as OED literature [[4](#), [7](#), [61](#)]. Consider heat transfer in a bounded two-dimensional domain  $\Omega$  depicted in [Figure 2](#). Suppose we have control over a source term  $z$  that acts within a particular subdomain  $\Omega_c \subset \Omega$ , which we refer to as the control region. Our goal is to steer the temperature distribution within  $\Omega$  by controlling the temperature within  $\Omega_c$ . To make matters

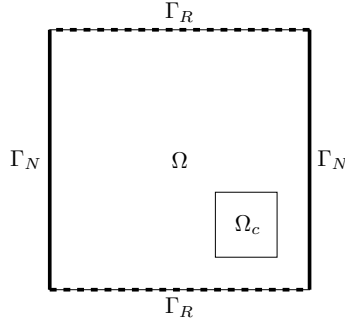


Figure 2: The domain of the heat transfer problem (2.3).

concrete, we assume the system is governed by the following advection diffusion equation.

$$\begin{aligned}
 (2.1) \quad & u_t - \kappa \Delta u + \mathbf{v} \cdot \nabla u = m + z \mathbb{1}_{\Omega_c} && \text{in } \Omega \times (0, T), \\
 & u(0, \mathbf{x}) = \hat{u}(\mathbf{x}; m) && \text{in } \Omega, \\
 & \nabla u \cdot \mathbf{n} = 0 && \text{on } \Gamma_N \times (0, T), \\
 & \nabla u \cdot \mathbf{n} = \gamma_h(u - \gamma_a) && \text{on } \Gamma_R \times (0, T).
 \end{aligned}$$

Here,  $\kappa$  is a diffusion constant,  $\mathbf{v}$  is a (steady) velocity field, and  $\gamma_h, \gamma_a$  are boundary coefficients. The system is fully insulated at  $\Gamma_N$ , and  $\Gamma_R$  experiences heat exchange from the ambient temperature  $\gamma_a$  with heat transfer rate  $\gamma_h$ .

Let us consider the volume source terms in (2.1). The first term,  $m$ , is an uncertain background source term, and the second one incorporates a control function  $z : [0, T] \rightarrow \mathbb{R}$ , where  $T$  is a final time. Here,  $\mathbb{1}_{\Omega_c}$  is the indicator function of the control region  $\Omega_c$ . We assume that we can control the temperature uniformly within  $\Omega_c$ . Furthermore,  $m$  is assumed to be a function  $m : \Omega \rightarrow \mathbb{R}$  that does not depend on time. Therefore, the combined source term in (2.1) is the function  $(\mathbf{x}, t) \mapsto m(\mathbf{x}) + \mathbb{1}_{\Omega_c}(\mathbf{x})z(t)$ . Note that the initial state  $\hat{u}$  is also parameterized by  $m$ . This is made precise shortly.

The optimal control problem seeks to steer the state  $u$  towards a target state  $\bar{u}$  by time  $T$ . This is done by finding  $u$  that solves

$$(2.2) \quad \min_{z \in L^2[0, T]} \Phi(z; m) := \frac{1}{2} \int_{\Omega} (u(\cdot, T) - \bar{u})^2 d\mathbf{x} + \frac{\beta}{2} \int_0^T z(t)^2 dt,$$

where  $u$  is the solution of the problem (2.1) and  $\beta > 0$  is a regularization parameter.

We next discuss the uncertain source term  $m$  in the above optimal control problem. We assume that the temperature distribution within the room is in steady state before the initial time,  $t = 0$ . Specifically, we assume that the initial temperature distribution  $\hat{u}$  satisfies

$$\begin{aligned}
 (2.3) \quad & -\kappa \Delta \hat{u} = m && \text{in } \Omega, \\
 & \nabla \hat{u} \cdot \mathbf{n} = 0 && \text{on } \Gamma_N, \\
 & \nabla \hat{u} \cdot \mathbf{n} = \gamma_h(\hat{u} - \gamma_a) && \text{on } \Gamma_R.
 \end{aligned}$$

This equation describes the (steady) temperature distribution, before applying temperature control in  $\Omega_c$ . Notably, the governing physics in (2.3) is different from that of (2.1).

As noted previously, the source term  $m$  is subject to uncertainty. We assume that we can reduce this uncertainty by solving an inverse problem. Suppose one can collect sensor measurements of temperature at a few sensors. We let  $\mathbf{y}$  denote the vector of measurements of  $\hat{u}$ . In what follows, we assume the following observation model,

$$(2.4) \quad \mathbf{y} = \hat{\mathcal{B}}\hat{u} + \boldsymbol{\eta}.$$

Here,  $\boldsymbol{\eta} \sim \mathcal{N}(\mathbf{0}, \mathbf{\Gamma}_{\text{noise}})$  models measurement noise and  $\hat{\mathcal{B}}$  is an observation operator that maps  $\hat{u}$  to the measurement space. Note that the mapping  $m \mapsto \hat{u}$  is an affine mapping of the form  $\hat{u} = \mathcal{S}m + s$ , where  $\mathcal{S}$  is a continuous linear transformation. We thus restate (2.4) as

$$(2.5) \quad \mathbf{y} = \mathcal{F}m + \mathbf{b} + \boldsymbol{\eta},$$

where  $\mathcal{F} := \hat{\mathcal{B}} \circ \mathcal{S}$  and  $\mathbf{b} := \hat{\mathcal{B}}s$ . Combining the present observation model with prior knowledge regarding  $m$ , we can formulate a Bayesian inverse problem for estimating  $m$ ; see Section 3.3.

As noted above, we use sensor measurements of  $\hat{u}$  to estimate  $m$ . Optimizing the placement of these sensors requires solving an OED problem; see Section 3.5 for background concepts regarding OED. However, since the estimation of  $m$  is only an intermediate step and the ultimate goal is solving the optimal control problem (2.2), a cOED approach is needed. In Section 4, we detail our proposed cOED formulation, for the class of problems under study.

**3. Preliminaries.** In this section, we discuss the necessary background for infinite-dimensional Bayesian inverse problems, optimal control, and design of experiments.

**3.1. Notation.** For a Hilbert space  $\mathcal{H}$ , we denote the inner product by  $\langle \cdot, \cdot \rangle_{\mathcal{H}}$  and the corresponding induced norm by  $\| \cdot \|_{\mathcal{H}}^2 = \langle \cdot, \cdot \rangle_{\mathcal{H}}$ . All Hilbert spaces considered in the present work are real separable Hilbert spaces. For two Hilbert spaces  $\mathcal{H}_1$  and  $\mathcal{H}_2$ , we denote the space of bounded linear transformations from  $\mathcal{H}_1$  to  $\mathcal{H}_2$  by  $\mathcal{L}(\mathcal{H}_1, \mathcal{H}_2)$  and the space of bounded linear operators on  $\mathcal{H}$  as  $\mathcal{L}(\mathcal{H})$ . We call  $\mathcal{A}^* \in \mathcal{L}(\mathcal{H}_2, \mathcal{H}_1)$  the adjoint of a linear operator  $\mathcal{A} \in \mathcal{L}(\mathcal{H}_1, \mathcal{H}_2)$  if it holds that  $\langle \mathcal{A}u, v \rangle_{\mathcal{H}_2} = \langle u, \mathcal{A}^*v \rangle_{\mathcal{H}_1}$  for all  $u \in \mathcal{H}_1$  and  $v \in \mathcal{H}_2$ . If  $\mathcal{A} \in \mathcal{L}(\mathcal{H})$  satisfies  $\mathcal{A} = \mathcal{A}^*$ , we call  $\mathcal{A}$  self-adjoint. We say that an operator  $\mathcal{A} \in \mathcal{L}(\mathcal{H})$  is positive if  $\langle x, \mathcal{A}x \rangle_{\mathcal{H}} \geq 0$  for all  $x \in \mathcal{H}$ , and  $\mathcal{A}$  is *strictly* positive, if  $\langle x, \mathcal{A}x \rangle_{\mathcal{H}} > 0$  for all nonzero  $x \in \mathcal{H}$ . Moreover, a positive self-adjoint  $\mathcal{A} \in \mathcal{L}(\mathcal{H})$  is said to be of trace-class if  $\text{tr}(\mathcal{A}) := \sum_{i=1}^{\infty} \langle \mathcal{A}e_i, e_i \rangle_{\mathcal{H}} < \infty$ , where  $\{e_i\}_{i=1}^{\infty}$  is any orthonormal basis of  $\mathcal{H}$ .

In what follows,  $\mathcal{N}(a, \mathcal{C})$  denotes a Gaussian measure with mean  $a$  and a strictly positive trace-class covariance operator  $\mathcal{C}$ . Also,  $\mathcal{U}$ ,  $\mathcal{Z}$ , and  $\mathcal{M}$  denote the Hilbert spaces corresponding to the state, control, and inversion parameters, respectively.

**3.2. Optimal control.** We consider optimal control problems of the form

$$(3.1a) \quad \min_{z \in \mathcal{Z}} \Phi(z; m) = \frac{1}{2} \|u(\cdot, T; m, z) - \bar{u}\|_{\mathcal{U}}^2 + \frac{\beta}{2} \|z\|_{\mathcal{Z}}^2,$$

where the state variable  $u \in \mathcal{U}$  satisfies

$$(3.1b) \quad \begin{aligned} \frac{du}{dt} &= \mathcal{L}u + \mathcal{C}z + \mathcal{D}m + c, \\ u(0) &= u_0. \end{aligned}$$

Here,  $z \in \mathcal{Z}$  is the control variable,  $u_0 \in \mathcal{U}$  is the initial state,  $m \in \mathcal{M}$  is an uncertain model parameter, and  $\beta > 0$  is a regularization parameter. In (3.1b),  $\mathcal{L}$ ,  $\mathcal{C}$ , and  $\mathcal{D}$  are linear operators, and  $c \in \mathcal{U}$  is an affine term. Note that subsequent developments can be extended in a straightforward manner to the cases of more general regularization operators.

Let  $u_T(m, z) = u(\cdot, T; m, z)$  denote the terminal state of  $u$ . This terminal state can be obtained via a mapping of the form

$$(3.2) \quad u_T(m, z) = \mathcal{A}m + \mathcal{B}z + q,$$

where  $\mathcal{A}$  and  $\mathcal{B}$  are linear transformations and  $q \in \mathcal{U}$ . We assume  $\mathcal{A} \in \mathcal{L}(\mathcal{M}, \mathcal{U})$  and  $\mathcal{B} \in \mathcal{L}(\mathcal{Z}, \mathcal{U})$ . We can thus restate the parameterized optimal control problem as

$$(3.3) \quad \min_{z \in \mathcal{Z}} \Phi(z; m) := \frac{1}{2} \|u_T(m, z) - \bar{u}\|_{\mathcal{U}}^2 + \frac{\beta}{2} \|z\|_{\mathcal{Z}}^2.$$

For a given  $m$ , the optimal control  $z_m^*$  solving (3.3) satisfies

$$\mathcal{H}_{\text{ctrl}} z_m^* = \mathcal{B}^*(\bar{u} - q - \mathcal{A}m), \quad \text{where} \quad \mathcal{H}_{\text{ctrl}} = \mathcal{B}^*\mathcal{B} + \beta I.$$

Therefore, in the present setting, we can express the optimal control as affine transformation of  $m$ ,  $z_m^* = -\mathcal{H}_{\text{ctrl}}^{-1} \mathcal{B}^* \mathcal{A}m + \mathcal{H}_{\text{ctrl}}^{-1} \mathcal{B}^*(\bar{u} - q)$ .

**3.3. Bayesian inverse problem.** In the present work, we consider inverse problems governed by observation models of the form

$$(3.4) \quad \mathbf{y} = \mathcal{F}m + \mathbf{b} + \boldsymbol{\eta}.$$

Here,  $\mathbf{y} \in \mathbb{R}^{n_y}$  is measurement data,  $\mathcal{F} : \mathcal{M} \rightarrow \mathbb{R}^{n_y}$  is a bounded linear transformation,  $\mathbf{b}$  is a constant vector, and  $\boldsymbol{\eta}$  is a random vector modeling measurement noise. Note that here we have an affine parameter-to-observable map,  $m \mapsto \mathcal{F}m + \mathbf{b}$ .

We assume  $\boldsymbol{\eta} \sim \mathcal{N}(\mathbf{0}, \mathbf{\Gamma}_{\text{noise}})$ , where  $\mathbf{\Gamma}_{\text{noise}} \in \mathbb{R}^{n_y \times n_y}$  represents the (symmetric positive definite) noise covariance matrix. Furthermore, we assume  $m$  and  $\boldsymbol{\eta}$  are independent random variables. We assume a Gaussian prior,  $\mu_{\text{pr}} = \mathcal{N}(m_{\text{pr}}, \mathcal{C}_{\text{pr}})$ , for the inversion parameter. Due to the affine structure of the parameter-to-observable map and the Gaussian assumption on the prior and noise models, the solution of the Bayesian inverse problem is the Gaussian posterior measure  $\mu_{\text{post}}^{\mathbf{y}} = \mathcal{N}(m_{\text{MAP}}, \mathcal{C}_{\text{post}})$  where

$$(3.5) \quad m_{\text{MAP}} = \mathcal{C}_{\text{post}} (\mathcal{F}^* \mathbf{\Gamma}_{\text{noise}}^{-1} (\mathbf{y} - \mathbf{b}) + \mathcal{C}_{\text{pr}}^{-1} m_{\text{pr}}) \quad \text{and} \quad \mathcal{C}_{\text{post}} = (\mathcal{F}^* \mathbf{\Gamma}_{\text{noise}}^{-1} \mathcal{F} + \mathcal{C}_{\text{pr}}^{-1})^{-1}.$$

**3.4. Discretization of control and inverse problems.** To facilitate computations, the inverse problem and the optimal control problem must be discretized. In this section, we briefly discuss the discretization of these problems.

**Discretization of Infinite-Dimensional Parameters.** We begin by considering the discretization of the inversion parameter. Herein, we assume the inversion parameter space is  $L^2(\Omega)$ , where  $\Omega$  is a bounded spatial domain. Let  $\widehat{\mathcal{M}}$  be a finite-dimensional subspace of  $\mathcal{M}$  spanned by continuous Lagrange nodal basis functions  $\{\phi_j\}_{j=1}^N$ . Then, any  $m \in \widehat{\mathcal{M}}$  can be

represented by the vector  $\mathbf{m} = [m_1 \cdots m_N]^\top$  of its expansion coefficients. Moreover, note that for every  $m, p \in \widehat{\mathcal{M}}$ ,

$$\langle m, p \rangle_{\mathcal{M}} = \sum_{i,j=1}^N m_i \langle \phi_i, \phi_j \rangle_{\mathcal{M}} p_j = \mathbf{m}^\top \mathbf{M} \mathbf{p} =: \langle \mathbf{m}, \mathbf{p} \rangle_{\mathbf{M}},$$

where  $\mathbf{M}$  denotes the finite-element mass matrix. Hence, we represent a discretized parameter  $\mathbf{m}$  in  $\mathbb{R}^N$  equipped with the weighted inner product  $\langle \cdot, \cdot \rangle_{\mathbf{M}}$ . We denote the inner product space  $(\mathbb{R}^N, \langle \cdot, \cdot \rangle_{\mathbf{M}})$  by  $\mathbb{R}_{\mathbf{M}}^N$ . The discretization of the target state  $u_T \in \mathcal{U}$  and the control variable  $z$  are done similarly. See [Appendix A](#), for details. We summarize the notations for the discretized inversion parameter, and the state and control variables in [Table 1](#).

Table 1: Discretization of the key quantities in inverse/optimal control problems. Here,  $\mathbb{R}_{\mathbf{M}}^N$ ,  $\mathbb{R}_{\mathbf{M}_z}^K$ , and  $\mathbb{R}_{\mathbf{M}_u}^L$  are, respectively,  $\mathbb{R}^N$ ,  $\mathbb{R}^K$ , and  $\mathbb{R}^L$  equipped with the respective weighted inner products and induced norms  $\|\cdot\|_{\mathbf{M}}$ ,  $\|\cdot\|_{\mathbf{M}_z}$ , and  $\|\cdot\|_{\mathbf{M}_u}$ .

Quantity	Functional notation	Discretization
inversion parameter	$m \in \mathcal{M}$	$\mathbf{m} \in \mathbb{R}_{\mathbf{M}}^N$
control variable	$z \in \mathcal{Z}$	$\mathbf{z} \in \mathbb{R}_{\mathbf{M}_z}^K$
target state	$u_T \in \mathcal{U}$	$\mathbf{u}_T \in \mathbb{R}_{\mathbf{M}_u}^L$

**Discretized Inverse Problem.** The discretized inverse problem seeks to estimate  $\mathbf{m}$  from the model,

$$(3.6) \quad \mathbf{y} = \mathbf{F} \mathbf{m} + \mathbf{b} + \boldsymbol{\eta},$$

given a data vector  $\mathbf{y} \in \mathbb{R}^{n_y}$ . Here,  $\mathbf{F} : \mathbb{R}_{\mathbf{M}}^N \rightarrow \mathbb{R}^{n_y}$  is the discretization of  $\mathcal{F}$  in [\(3.4\)](#). The corresponding posterior distribution for  $\mathbf{m}$  is given by  $\mu_{\text{post}}^{\mathbf{y}} = \mathcal{N}(\mathbf{m}_{\text{MAP}}, \boldsymbol{\Gamma}_{\text{post}})$ , where

$$(3.7) \quad \mathbf{m}_{\text{MAP}} = \boldsymbol{\Gamma}_{\text{post}} (\mathbf{F}^* \boldsymbol{\Gamma}_{\text{noise}}^{-1} (\mathbf{y} - \mathbf{b}) + \boldsymbol{\Gamma}_{\text{pr}}^{-1} \mathbf{m}_{\text{pr}}) \quad \text{and} \quad \boldsymbol{\Gamma}_{\text{post}} = (\mathbf{F}^* \boldsymbol{\Gamma}_{\text{noise}}^{-1} \mathbf{F} + \boldsymbol{\Gamma}_{\text{pr}}^{-1})^{-1}.$$

Note that here  $\boldsymbol{\Gamma}_{\text{pr}}$  is the discretized prior covariance operator and  $\mathbf{F}^*$  is the adjoint of  $\mathbf{F}$ . It is important to note that  $\mathbf{F}$  is a linear transformation from  $\mathbb{R}_{\mathbf{M}}^N$  to the measurement space, which is equipped with the Euclidean inner product. This implies  $\mathbf{F}^* = \mathbf{M}^{-1} \mathbf{F}^\top$ . See [\[14\]](#) for further details regarding discretization of infinite-dimensional Bayesian inverse problems.

**Discretized Optimal Control Problem.** We consider

$$(3.8a) \quad \min_{\mathbf{z} \in \mathbb{R}_{\mathbf{M}_z}^K} \Phi(\mathbf{z}; \mathbf{m}) := \frac{1}{2} \|\mathbf{u}(T) - \bar{\mathbf{u}}\|_{\mathbf{M}_u}^2 + \frac{\beta}{2} \|\mathbf{z}\|_{\mathbf{M}_z}^2,$$

where the state variable  $\mathbf{u}$  satisfies

$$(3.8b) \quad \begin{aligned} \frac{d\mathbf{u}}{dt} &= \mathbf{L} \mathbf{u} + \mathbf{C} \mathbf{z} + \mathbf{D} \mathbf{m} + \mathbf{c}, \\ \mathbf{u}(0) &= \mathbf{u}_0. \end{aligned}$$

Here,  $\mathbf{z}$  is the discretized control variable,  $\mathbf{u}_0$  is the discretized initial condition, and  $\mathbf{m}$  is the discretized inversion parameter. Here,  $\mathbf{L}$ ,  $\mathbf{C}$  and  $\mathbf{D}$  are (finite-dimensional) linear operators, and  $\mathbf{c} \in \mathbb{R}_{\mathbf{M}_u}^L$  is an affine term pertaining to the prediction model. Note that the terminal state,  $\mathbf{u}_T := \mathbf{u}(T)$ , is obtained via a mapping of the form

$$(3.9) \quad \mathbf{u}_T(\mathbf{m}, \mathbf{z}) = \mathbf{A}\mathbf{m} + \mathbf{B}\mathbf{z} + \mathbf{q},$$

where  $\mathbf{A} \in \mathcal{L}(\mathbb{R}_{\mathbf{M}}^N, \mathbb{R}_{\mathbf{M}_u}^L)$ ,  $\mathbf{B} \in \mathcal{L}(\mathbb{R}_{\mathbf{M}_z}^K, \mathbb{R}_{\mathbf{M}_u}^L)$ , and  $\mathbf{q} \in \mathbb{R}_{\mathbf{M}_u}^L$ . We also need the adjoints of  $\mathbf{A}$  and  $\mathbf{B}$  in what follows. It is simple to note that  $\mathbf{A}^* = \mathbf{M}^{-1}\mathbf{A}^\top \mathbf{M}_u$  and  $\mathbf{B}^* = \mathbf{M}_z^{-1}\mathbf{B}^\top \mathbf{M}_u$ .

Restating the parameterized optimal control problem as

$$(3.10) \quad \min_{\mathbf{z} \in \mathbb{R}_{\mathbf{M}_z}^K} \Phi(\mathbf{z}; \mathbf{m}) = \frac{1}{2} \|\mathbf{u}_T(\mathbf{m}, \mathbf{z}) - \bar{\mathbf{u}}\|_{\mathbf{M}_u}^2 + \frac{\beta}{2} \|\mathbf{z}\|_{\mathbf{M}_z}^2,$$

we note that the optimal control  $\mathbf{z}_m^*$ , corresponding to a fixed  $\mathbf{m}$ , satisfies

$$\mathbf{H}_{\text{ctrl}} \mathbf{z}_m^* = \mathbf{B}^*(\bar{\mathbf{u}} - \mathbf{q} - \mathbf{A}\mathbf{m}), \quad \text{where} \quad \mathbf{H}_{\text{ctrl}} = \mathbf{B}^*\mathbf{B} + \beta\mathbf{M}_z.$$

We can therefore express the optimal control  $\mathbf{z}_m^*$  as

$$(3.11) \quad \mathbf{z}_m^* := -\mathbf{H}_{\text{ctrl}}^{-1} \mathbf{B}^* \mathbf{A} \mathbf{m} + \mathbf{H}_{\text{ctrl}}^{-1} \mathbf{B}^* (\bar{\mathbf{u}} - \mathbf{q}).$$

Recall that the inversion parameter  $\mathbf{m}$  is unknown and is modeled as a random variable. A useful estimate of this parameter is given by the MAP point  $\mathbf{m}_{\text{MAP}}$ ; see (3.7). In particular, this yields a nominal optimal control  $\mathbf{z}^* := \mathbf{z}_{\mathbf{m}_{\text{MAP}}}^*$ . This provides an estimate for the optimal control that reflects the *best-guess* inversion parameter and is the control that we would recommend to a practitioner to implement.

**3.5. Optimal experimental design (OED).** We formulate the OED problem as that of selecting an optimal subset from a set  $\{\mathbf{x}_i\}_{i=1}^{n_s}$  of candidate locations for placing sensors. To facilitate this, we assign a binary weight  $w_i \in \{0, 1\}$  to each candidate location. Sensors are placed at locations whose corresponding weight is one. In this setting, an experimental design is fully specified by a weight vector  $\mathbf{w} = [w_1 \cdots w_{n_s}]^\top \in \{0, 1\}^{n_s}$ . In what follows, we assume the sensor measurements are uncorrelated and let  $\mathbf{\Gamma}_{\text{noise}} = \sigma^2 \mathbf{I}$  for convenience. Note that it is possible to extend the subsequent theory and derivations in a straightforward manner for the case of correlated noise.

Before formulating an OED problem, we need to specify how an experimental design is incorporated in the Bayesian inverse problem. Following the formulations in [3], we consider the design-dependent posterior distribution  $\mathcal{N}(\mathbf{m}_{\text{MAP}}(\mathbf{w}, \mathbf{y}), \mathbf{\Gamma}_{\text{post}}(\mathbf{w}))$ , where

$$(3.12) \quad \mathbf{m}_{\text{MAP}}(\mathbf{w}, \mathbf{y}) = \mathbf{\Gamma}_{\text{post}} (\mathbf{F}^* \mathbf{W}_\sigma (\mathbf{y} - \mathbf{b}) + \mathbf{\Gamma}_{\text{pr}}^{-1} \mathbf{m}_{\text{pr}}), \quad \mathbf{\Gamma}_{\text{post}}(\mathbf{w}) = (\mathbf{F}^* \mathbf{W}_\sigma \mathbf{F} + \mathbf{\Gamma}_{\text{pr}}^{-1})^{-1},$$

where  $\mathbf{W}_\sigma := \sigma^{-2} \text{diag}(\mathbf{w})$ . Note that whereas  $\mathbf{m}_{\text{MAP}}$  depends on measurement data, the posterior covariance  $\mathbf{\Gamma}_{\text{post}}$  depends only on the design  $\mathbf{w}$ . Note also that

$$(3.13) \quad \mathbf{\Gamma}_{\text{post}}(\mathbf{w}) = \mathbf{\Gamma}_{\text{pr}}^{1/2} (\tilde{\mathbf{H}}_{\text{misfit}}(\mathbf{w}) + \mathbf{I})^{-1} \mathbf{\Gamma}_{\text{pr}}^{1/2},$$

where  $\tilde{\mathbf{H}}_{\text{misfit}}(\mathbf{w})$  is the *prior-preconditioned* data misfit Hessian [14] defined as,

$$(3.14) \quad \tilde{\mathbf{H}}_{\text{misfit}}(\mathbf{w}) = \mathbf{\Gamma}_{\text{pr}}^{1/2} (\mathbf{F}^* \mathbf{W}_\sigma \mathbf{F}) \mathbf{\Gamma}_{\text{pr}}^{1/2}.$$

In ill-posed inverse problems with sparse data  $\tilde{\mathbf{H}}_{\text{misfit}}$  can often be represented accurately with a low-rank approximation. This plays a key role in the computational methods in Section 5.

The OED problem seeks to minimize a design criterion  $\Psi(\mathbf{w})$  over the set  $\{\mathbf{w} \in \{0, 1\}^{n_s} : \sum_{i=1}^{n_s} w_i = k\}$ , where  $k$  is a sensor budget. Note that the design criterion cannot be dependent on a specific realization of data, as experimental data is not available *a priori* at the stage of solving an OED problem. In traditional Bayesian OED, one typically considers design criteria that quantify measures of posterior uncertainty in the inversion parameter or information gain. An example is the A-optimality criterion

$$(3.15) \quad \Psi^A(\mathbf{w}) := \text{tr}[\mathbf{\Gamma}_{\text{post}}(\mathbf{w})],$$

which quantifies the average posterior variance of the inversion parameter.

**4. Control-oriented design criterion and uncertainty quantification.** In this section, we present our proposed mathematical framework for control-oriented OED (cOED) and uncertainty quantification in parameterized optimal control problems. We begin by deriving our proposed cOED criterion in Section 4.1. Subsequently, in Section 4.2, we characterize the first and second moments of the optimal control objective and derive a concentration bound for this quantity. The latter analysis connects the proposed cOED criterion to the tail probabilities of the optimal control objective.

**4.1. A control-oriented design criterion.** Let us consider how the posterior uncertainty in the inversion parameter propagates to the optimal terminal state, i.e., the terminal state (3.9) evaluated at the optimal control. Upon parameter inversion, we obtain a posterior  $\mu_{\text{post}}^y = \mathcal{N}(\mathbf{m}_{\text{MAP}}^y, \mathbf{\Gamma}_{\text{post}})$  as defined in (3.12). The resulting MAP parameter estimate,  $\mathbf{m}_{\text{MAP}}^y$ , is then used to compute a nominal optimal control  $\mathbf{z}^*$  (3.11). We apply this control to the system (3.9), which results in the optimal terminal state,

$$(4.1) \quad \mathbf{u}_T^*(\mathbf{m}) := \mathbf{A}\mathbf{m} + \mathbf{B}\mathbf{z}^* + \mathbf{q}.$$

The goal of optimal control is to guide  $\mathbf{u}_T^*(\mathbf{m})$  towards the target state  $\bar{\mathbf{u}}$ . However, the terminal state of the system,  $\mathbf{u}_T^*(\mathbf{m})$ , itself is uncertain due to uncertainty in  $\mathbf{m}$ . We can use the posterior distribution  $\mu_{\text{post}}^y$  of  $\mathbf{m}$  to obtain a probabilistic depiction of the terminal state. Specifically, we have

$$(4.2) \quad \mathbf{u}_T^* \sim \mathcal{N}(\mathbf{u}_T^*(\mathbf{m}_{\text{MAP}}^y), \mathbf{A}\mathbf{\Gamma}_{\text{post}}\mathbf{A}^*).$$

In a control-oriented application, it is important to reduce uncertainty in  $\mathbf{u}_T^*$ . Following a weighted A-optimal design approach, we define the cOED criterion as

$$(4.3) \quad \Psi^{cA} := \text{tr}(\mathbf{A}\mathbf{\Gamma}_{\text{post}}\mathbf{A}^*).$$

This criterion quantifies the *average* variance in the terminal state  $\mathbf{u}_T^*(\mathbf{m})$ . Note that this coincides with the average posterior variance of  $\mathbf{u}_T^* - \bar{\mathbf{u}}$ . Therefore, the cOED criterion is also

representative of uncertainty in the deviation of the terminal state from the target state. It is worth noting that there exist different ways of equivalently expressing the posterior covariance of  $\mathbf{u}_T^*$  [54, 61]. Moreover, one can also view the cOED criterion from a decision-theoretic perspective as the expected Bayes Risk of  $\mathbf{u}_T^*$ :

$$(4.4) \quad \Psi^{cA} = \text{tr}(\mathbf{A}\mathbf{\Gamma}_{\text{post}}\mathbf{A}^*) = \mathbb{E}_{\mu_{\text{pr}}} \left\{ \mathbb{E}_{\mathbf{y}|\mathbf{m}} \left[ \|\mathbf{u}_T^*(\mathbf{m}_{\text{MAP}}^{\mathbf{y}}) - \mathbf{u}_T^*(\mathbf{m})\|_{\mathbf{M}_u}^2 \right] \right\},$$

The proof of this relation is given in [9, Theorem 3.1]. Thus, the cOED criterion also quantifies the expectation, over the set of all likely data, of the mean-squared deviation of the optimal terminal state. For further details on the concept of Bayes risk, see, e.g., [57, Page 87].

**4.2. Measures of uncertainty in the control objective.** Upon solving the cOED problem, we obtain a sensor placement. Then, we can solve the inverse problem to estimate the inversion parameter  $\mathbf{m}$ . Subsequently, the MAP estimate of  $\mathbf{m}$  can be used to solve the optimal control problem. A key downstream consideration is characterizing the uncertainty in the optimal control objective. In particular, we consider the uncertainty in the (non-regularized) control objective,

$$(4.5) \quad \Phi_{\text{ctrl}}^*(\mathbf{m}) := \frac{1}{2} \|\mathbf{u}_T^*(\mathbf{m}) - \bar{\mathbf{u}}\|_{\mathbf{M}_u}^2 = \frac{1}{2} \|\mathbf{A}\mathbf{m} + \mathbf{B}\mathbf{z}^* + \mathbf{q} - \bar{\mathbf{u}}\|_{\mathbf{M}_u}^2.$$

Note that  $\Phi_{\text{ctrl}}^*$  is a quadratic functional of a Gaussian random variable. This enables efficient sampling and theoretical analysis of this quantity. In Section 4.2.1, we derive the expressions for the expectation and variance of the control objective and relate these expressions to the cOED criterion. Also, in Section 4.2.2, we derive a concentration bound that characterizes uncertainty in the control objective in terms of  $\Psi^{cA}$ . These results provide a framework for quantitatively and qualitatively assessing the uncertainty in the control objective.

**4.2.1. Expectation and Variance of  $\Phi_{\text{ctrl}}^*$ .** We begin by presenting the expressions for the mean and variance of the control objective with respect to the posterior law  $\mu_{\text{post}}^{\mathbf{y}} = \mathcal{N}(\mathbf{m}_{\text{MAP}}, \mathbf{\Gamma}_{\text{post}})$  of  $\mathbf{m}$ , whose mean and covariance are defined in (3.7).

**Proposition 4.1.** *Let  $\mathbb{E}(\cdot | \mathbf{y})$  and  $\text{Var}(\cdot | \mathbf{y})$  denote expectation and variance with respect to  $\mu_{\text{post}}^{\mathbf{y}}$ . We have*

$$(4.6a) \quad \mathbb{E}(\Phi_{\text{ctrl}}^* | \mathbf{y}) = \frac{1}{2} \text{tr}[\mathbf{A}\mathbf{\Gamma}_{\text{post}}\mathbf{A}^*] + \frac{1}{2} \|\mathbf{A}\mathbf{m}_{\text{MAP}}^{\mathbf{y}} + \mathbf{B}\mathbf{z}^* + \mathbf{q} - \bar{\mathbf{u}}\|_{\mathbf{M}_u}^2,$$

$$(4.6b) \quad \text{Var}(\Phi_{\text{ctrl}}^* | \mathbf{y}) = \frac{1}{2} \text{tr}[(\mathbf{A}\mathbf{\Gamma}_{\text{post}}\mathbf{A}^*)^2] + \|\mathbf{A}\mathbf{m}_{\text{MAP}}^{\mathbf{y}} + \mathbf{B}\mathbf{z}^* + \mathbf{q} - \bar{\mathbf{u}}\|_{\mathbf{M}_u \mathbf{A} \mathbf{\Gamma}_{\text{post}} \mathbf{A}^*}^2.$$

*Note that  $\mathbf{z}^*$  depends on  $\mathbf{m}_{\text{MAP}}$ , whose dependence on  $\mathbf{y}$  is highlighted as  $\mathbf{m}_{\text{MAP}}^{\mathbf{y}}$  for clarity.*

*Proof.* See Appendix B.1. ■

Using Proposition 4.1, one can quantitatively estimate the expected error in the terminal state, having applied the nominal optimal control corresponding to the MAP point. Note that (4.6a) can be restated in terms of the control-oriented design criterion,  $\Psi^{cA}$ , as

$$(4.7) \quad \mathbb{E}(\Phi_{\text{ctrl}}^* | \mathbf{y}) = \frac{1}{2} [\Psi^{cA} + \Phi_{\text{ctrl}}^*(\mathbf{m}_{\text{MAP}}^{\mathbf{y}})].$$

This suggests that minimization of the control-oriented criterion can potentially reduce the expected control objective. However, due to the dependence of (4.7) on data, minimization of  $\Psi^{cA}$  may not guarantee minimization of  $\mathbb{E}(\Phi_{\text{ctrl}}^* | \mathbf{y})$ . Nevertheless, in the case where the variance of  $\Psi^{cA}$  over designs dominates  $\Phi_{\text{ctrl}}^*(\mathbf{m}_{\text{MAP}}^{\mathbf{y}})$ , the expectation and variance of the control objective is often minimized with a cOED.

We also note that the cOED criterion can be bounded by the classical A-optimality criterion (3.15). Namely, it is straightforward to show that

$$\frac{|\Psi^{cA} - \Psi^A|}{\Psi^A} \leq \|\mathbf{A}^* \mathbf{A} - \mathbf{I}\|,$$

where the norm in the right-hand side is the operator norm induced by the norm  $\|\cdot\|_{\mathbf{M}}$  on  $\mathbb{R}_{\mathbf{M}}^N$ ; see [11, Fact 5.12.7]. As a result, in situations where  $\mathbf{A}$  has near-orthogonal columns, minimizing the classical A-optimality criterion can be beneficial in terms of reducing the cOED criterion. This, however, does not hold in general, where  $\|\mathbf{A}^* \mathbf{A} - \mathbf{I}\|$  might be large.

**4.2.2. Concentration Bounds for  $\Phi_{\text{ctrl}}^*$ .** In practical settings, it is often of interest to gauge the probability of a *worst-case* scenario, i.e., the case where the nominal control yields an unexpectedly large control objective. Here, we analyze the probability of deviations of the control objective from its expectation and demonstrate the advantages of a control-oriented design in this aspect. The following result Proposition 4.2 and the subsequent corollary provide insight into this.

**Proposition 4.2 (Concentration bound for  $\Phi_{\text{ctrl}}^*$ ).** *For every  $\tau \geq 0$ ,*

$$(4.8) \quad \mathbb{P}(|\Phi_{\text{ctrl}}^*(\mathbf{m}) - \mathbb{E}(\Phi_{\text{ctrl}}^* | \mathbf{y})| \geq \tau) \leq 4 \exp \left[ -\frac{1}{8} \min \left\{ \frac{\tau}{\Psi^{cA}}, \frac{\tau^2}{(\Psi^{cA})^2}, \frac{\tau^2}{C^2} \right\} \right],$$

where  $C = \|\mathbf{A}\mathbf{m}_{\text{MAP}} + \mathbf{B}\mathbf{z}^* + \mathbf{q} - \bar{\mathbf{u}}\|_{\mathbf{M}_{\mathbf{u}}\mathbf{A}\mathbf{\Gamma}_{\text{post}}\mathbf{A}^*}$ .

*Proof.* See Appendix B.2. ■

**Corollary 4.3.** *Consider the setup from Proposition 4.2. Let  $0 < \delta < 1$ . Then, with probability of at least  $1 - \delta$ ,*

$$(4.9) \quad |\Phi_{\text{ctrl}}^*(\mathbf{m}) - \mathbb{E}(\Phi_{\text{ctrl}}^* | \mathbf{y})| \leq \sqrt{8 \log(4/\delta)} \max \left\{ \sqrt{8 \log(4/\delta)} \Psi^{cA}, \Psi^{cA}, C \right\},$$

where  $C$  is as defined in Proposition 4.2.

*Proof.* See Appendix B.2. ■

Note that for large deviations  $\tau$ , the concentration bound (4.8) behaves like  $\exp(-\tau/\Psi^{cA})$ . In other words, the probability of the control objective being much larger than its expectation (i.e., probability of a worst-case scenario) is restricted by  $\Psi^{cA}$ . Similarly, Corollary 4.3 shows that the size of high-probability confidence regions for the control objective is proportional to  $\Psi^{cA}$ . Based on these observations, it is expected that an experimental design minimizing the control-oriented criterion  $\Psi^{cA}$  would aid in reducing uncertainty in the control objective. Computational results in Section 6.4.2 provide further intuition for the established relationship between the expectation and variance of  $\Phi_{\text{ctrl}}^*$  and the cOED criterion.

**5. Computational methods.** In this section, we discuss the computational methods used for solving the control-oriented OED (cOED) problem and quantifying the uncertainty in the control objective. We rely on a greedy approach for approximately solving the cOED problem; see [Section 5.1](#). Such optimization routines involve repeated evaluations of the cOED criterion. Hence, efficient estimation of the cOED criterion is essential. In [Section 5.2](#), we outline fast computational methods for computing this criterion. Then, in [Section 5.3](#) we discuss fast computation of measures of uncertainty in the control objective.

**5.1. Greedy sensor placement.** To find an optimal sensor placement, we need to minimize the cOED criterion given a fixed budget  $k$  of sensors. Solving this combinatorial optimization problem via exhaustive search is computationally intractable in practice. A practical approach for approximately solving this problem is to use a greedy procedure; see [Algorithm 5.1](#). In this approach, sensors are selected by successively identifying a candidate sensor location in each stage that locally minimizes the design criterion. Note that the minimizer in line 3 of [Algorithm 5.1](#) may not be unique, in which case, we arbitrarily select one of the minimizers.

Despite being suboptimal, the greedy approach can provide useful designs in practice, and its effectiveness has been analyzed rigorously in the context of experimental design [\[12, 38\]](#). In place of the greedy algorithm, one may also consider exchange algorithms [\[32\]](#), relaxation approaches [\[3\]](#), stochastic binary optimization [\[10\]](#), or other heuristic methods for optimization [\[36\]](#). Note that [Algorithm 5.1](#) still requires many evaluations of the criterion, roughly in the order of  $kn_s$ . Hence, efficient computation of the design criterion is critical to the feasibility of the method, which we address next.

---

**Algorithm 5.1** Greedy Sensor Placement

---

**Input:** Target number of sensors  $k \leq n_s$  and design criterion  $\Psi : \mathbf{w} \mapsto \Psi(\mathbf{w}) \in \mathbb{R}^+$

**Output:** Design vector  $\mathbf{w} \in \mathbb{R}^{n_s}$

- 1: Set  $\mathbf{w} = \mathbf{0}$ ,  $\mathcal{U} = \{1, \dots, n_s\}$ , and  $\mathcal{S} = \emptyset$
  - 2: **for**  $i = 1, 2, \dots, k$  **do**
  - 3:    $i^* = \arg \min_{j \in \mathcal{U} \setminus \mathcal{S}} \Psi(\mathbf{w} + \mathbf{e}_j)$
  - 4:    $\mathcal{S} = \mathcal{S} \cup \{i^*\}$
  - 5:    $\mathbf{w} = \mathbf{w} + \mathbf{e}_{i^*}$
  - 6: **end for**
- 

**5.2. Efficient estimation of cOED criterion.** Consider the control-oriented A-optimal criterion from [\(4.3\)](#):

$$(5.1) \quad \Psi^{cA} = \text{tr}(\mathbf{A}\mathbf{\Gamma}_{\text{post}}\mathbf{A}^*) = \sum_{i=1}^L \langle \mathbf{A}\mathbf{\Gamma}_{\text{post}}\mathbf{A}^* \mathbf{e}_i, \mathbf{e}_i \rangle_{\mathbf{M}_u},$$

where  $\{\mathbf{e}_i\}_{i=1}^L$  is an orthonormal basis of  $\mathbb{R}_{\mathbf{M}_u}^L$ . Direct computation of [\(5.1\)](#) requires  $L$  matrix vector products with  $\mathbf{\Gamma}_{\text{post}}$ . This is prohibitively expensive in practice—the discretized parameter dimension is typically on the order of thousands or tens of thousands. Moreover, computing an application of  $\mathbf{\Gamma}_{\text{post}}$  using an iterative method (e.g., CG or an appropriate Krylov subspace method) is expensive due to the need for repeated applications of  $\mathbf{F}$  and  $\mathbf{F}^*$ ,

i.e., forward and adjoint PDE solves. Note also that evaluating the trace in (5.1) requires  $L$  matrix-vector products with the adjoint of the goal-operator  $\mathbf{A}$ ; i.e.,  $L$  additional PDE solves. This section is about addressing these challenges.

We first discuss fast methods for computing applications of  $\mathbf{\Gamma}_{\text{post}}$  on vectors. Two approaches are considered. The first one, which we refer to as the *spectral approach*, relies on a low-rank spectral decomposition of the prior-preconditioned data-misfit Hessian. The second approach, which we call the *frozen low-rank forward operator approach*, uses a low-rank SVD of the prior-preconditioned forward operators. As we will see, the latter approach has the benefit of being design-independent and therefore is more suitable for our purposes.

**5.2.1. Fast  $\mathbf{\Gamma}_{\text{post}}$  apply using the spectral approach.** As noted previously, the prior-preconditioned Hessian (3.14) often can be represented accurately using a low-rank spectral decomposition:

$$(5.2) \quad \tilde{\mathbf{H}}_{\text{misfit}} \approx \mathbf{V}_h \mathbf{\Lambda} \mathbf{V}_h^*.$$

Here,  $\mathbf{\Lambda} \in \mathbb{R}^{k_h \times k_h}$  is a diagonal matrix with the leading eigenvalues of  $\tilde{\mathbf{H}}_{\text{misfit}}$  on its diagonal and  $\mathbf{V}_h \in \mathcal{L}(\mathbb{R}^{k_h}, \mathbb{R}_M^N)$  satisfies  $\mathbf{V}_h^* \mathbf{V}_h = \mathbf{I}$ , where  $\mathbf{V}_h^* = \mathbf{V}_h^\top \mathbf{M}$ . This decomposition can be obtained iteratively using the Lanczos method [43] or through approximation techniques such as a randomized Nyström decomposition [25]. This generally requires at least  $k_h$  applications of  $\mathbf{F}$  and its adjoint  $\mathbf{F}^*$ . Note that the data-misfit Hessian (5.2) and its low-rank approximation depend on the design vector  $\mathbf{w}$  by (3.14). Moreover, by (3.14), it follows that the rank of the data-misfit Hessian does not exceed  $n_s$ .

Once the low-rank approximation (5.2) is available, we can use the Sherman-Morrison-Woodbury identity [29] to obtain

$$(\tilde{\mathbf{H}}_{\text{misfit}} + \mathbf{I})^{-1} \approx (\mathbf{V}_h \mathbf{\Lambda} \mathbf{V}_h^* + \mathbf{I})^{-1} = \mathbf{I} - \mathbf{V}_h \mathbf{D} \mathbf{V}_h^*,$$

where  $\mathbf{D} := \text{diag}(\lambda_1/(\lambda_1 + 1), \lambda_2/(\lambda_2 + 1), \dots, \lambda_{k_h}/(\lambda_{k_h} + 1))$ . This yields the following approximation for the posterior covariance,

$$(5.3) \quad \mathbf{\Gamma}_{\text{post}} \approx \tilde{\mathbf{\Gamma}}_{\text{post,h}} := \mathbf{\Gamma}_{\text{pr}} - \mathbf{\Gamma}_{\text{pr}}^{1/2} \mathbf{V}_h \mathbf{D} \mathbf{V}_h^* \mathbf{\Gamma}_{\text{pr}}^{1/2}.$$

This approximation of  $\mathbf{\Gamma}_{\text{post}}$  has been used in various previous studies in Bayesian analysis and OED; see, e.g., [6, 14].

**5.2.2. Fast  $\mathbf{\Gamma}_{\text{post}}$  apply using the frozen low-rank forward operator approach.** Consider the  $\mathbf{w}$ -dependent prior-preconditioned data-misfit Hessian

$$\tilde{\mathbf{H}}_{\text{misfit}}(\mathbf{w}) = \mathbf{\Gamma}_{\text{pr}}^{1/2} \mathbf{F}^* \mathbf{W}_\sigma \mathbf{F} \mathbf{\Gamma}_{\text{pr}}^{1/2} = \tilde{\mathbf{F}}^* \mathbf{W}_\sigma \tilde{\mathbf{F}}.$$

Here,  $\tilde{\mathbf{F}} := \mathbf{F} \mathbf{\Gamma}_{\text{pr}}^{1/2}$  is the prior-preconditioned forward operator. We utilize the generalized randomized SVD algorithm [30, 53] with target rank  $k_f$  and modest oversampling parameter ( $p = 5$ ) to compute  $\tilde{\mathbf{F}} \approx \mathbf{U}_F \mathbf{V}_F^*$ , where  $\mathbf{U}_F \in \mathbb{R}^{n_y \times k_f}$  is a matrix with orthonormal columns, and  $\mathbf{V}_F \in \mathcal{L}(\mathbb{R}^{k_f}, \mathbb{R}_M^N)$  encodes the right singular vectors and singular values. Substituting this approximation into (3.13) yields

$$\mathbf{\Gamma}_{\text{post}} \approx \tilde{\mathbf{\Gamma}}_{\text{post,f}} := \mathbf{\Gamma}_{\text{pr}}^{1/2} \left( \mathbf{V}_F \mathbf{U}_F^\top \mathbf{W}_\sigma \mathbf{U}_F \mathbf{V}_F^* + \mathbf{I} \right)^{-1} \mathbf{\Gamma}_{\text{pr}}^{1/2}.$$

For notational convenience, we define  $\mathbf{C}_w \in \mathbb{R}^{k_f \times k_f}$  by

$$(5.4) \quad \mathbf{C}_w := \mathbf{U}_F^\top \mathbf{W}_\sigma \mathbf{U}_F,$$

and use  $\tilde{\mathbf{\Gamma}}_{\text{post},f} = \mathbf{\Gamma}_{\text{pr}}^{1/2} (\mathbf{V}_F \mathbf{C}_w \mathbf{V}_F^* + \mathbf{I})^{-1} \mathbf{\Gamma}_{\text{pr}}^{1/2}$ . Using the Sherman-Morrison-Woodbury identity, we have  $(\mathbf{V}_F \mathbf{C}_w \mathbf{V}_F^* + \mathbf{I})^{-1} = \mathbf{I} - \mathbf{V}_F (\mathbf{C}_w \mathbf{V}_F^* \mathbf{V}_F + \mathbf{I})^{-1} \mathbf{C}_w \mathbf{V}_F^*$ . Therefore,

$$(5.5) \quad \tilde{\mathbf{\Gamma}}_{\text{post},f} = \mathbf{\Gamma}_{\text{pr}} - \mathbf{\Gamma}_{\text{pr}}^{1/2} [\mathbf{V}_F (\mathbf{C}_w \mathbf{V}_F^* \mathbf{V}_F + \mathbf{I})^{-1} \mathbf{C}_w \mathbf{V}_F^*] \mathbf{\Gamma}_{\text{pr}}^{1/2}.$$

Note that as opposed to (3.13), which involves the inverse of an operator in  $\mathbb{R}^{N \times N}$ , (5.5) only requires the inverse of a matrix in  $\mathbb{R}^{k_f \times k_f}$ . In practice, typically,  $k_f$  is much smaller than the discretized parameter dimension  $N$ . Moreover, once the discretization of the problem is sufficiently fine to resolve the dominant singular values of  $\tilde{\mathbf{F}}$ , the numerical rank  $k_f$  does not grow upon successive mesh refinements.

**5.2.3. Fast computation of the cOED criterion.** The frozen low-rank forward operator approach discussed above is particularly well-suited to the present Bayesian inverse problem setup. Thus, we first present a procedure for fast computation of the cOED criterion using this approach. As seen shortly, at the up-front cost of precomputing the low-rank approximation of  $\tilde{\mathbf{F}}$ , we can solve the cOED optimization problem with no need for  $\mathbf{F}$  and  $\mathbf{F}^*$  applies, which require forward and adjoint PDE solves. Moreover, by precomputing  $k_f$  applications of the goal operator  $\mathbf{A}$ , the cOED criterion can be estimated with no additional solves of the PDEs governing the optimal control problem or the corresponding adjoint PDEs. It is noteworthy that access to the adjoint of the goal operator,  $\mathbf{A}^*$ , is not required in this approach.

Using the low-rank SVD of  $\tilde{\mathbf{F}}$ , we obtain the approximation

$$\Psi^{cA} = \text{tr}(\mathbf{A} \mathbf{\Gamma}_{\text{post}} \mathbf{A}^*) \approx \text{tr}(\mathbf{A} \tilde{\mathbf{\Gamma}}_{\text{post},f} \mathbf{A}^*) =: \tilde{\Psi}_{\text{f}}^{cA}.$$

Substituting the expression from (5.5), we have

$$\begin{aligned} \mathbf{A} \tilde{\mathbf{\Gamma}}_{\text{post},f} \mathbf{A}^* &= \mathbf{A} \left( \mathbf{\Gamma}_{\text{pr}} - \mathbf{\Gamma}_{\text{pr}}^{1/2} [\mathbf{V}_F (\mathbf{C}_w \mathbf{V}_F^* \mathbf{V}_F + \mathbf{I})^{-1} \mathbf{C}_w \mathbf{V}_F^*] \mathbf{\Gamma}_{\text{pr}}^{1/2} \right) \mathbf{A}^* \\ &= \mathbf{A} \mathbf{\Gamma}_{\text{pr}} \mathbf{A}^* - \tilde{\mathbf{A}} (\mathbf{C}_w \mathbf{V}_F^* \mathbf{V}_F + \mathbf{I})^{-1} \mathbf{C}_w \tilde{\mathbf{A}}^*, \end{aligned}$$

where  $\tilde{\mathbf{A}} := \mathbf{A} \mathbf{\Gamma}_{\text{pr}}^{1/2} \mathbf{V}_F$ . A straightforward algebraic manipulation yields

$$(5.6) \quad \tilde{\Psi}_{\text{f}}^{cA} = \text{tr}(\mathbf{A} \tilde{\mathbf{\Gamma}}_{\text{post},f} \mathbf{A}^*) = \text{tr}(\mathbf{A} \mathbf{\Gamma}_{\text{pr}} \mathbf{A}^*) - \text{tr} \left[ (\mathbf{C}_w \mathbf{V}_F^* \mathbf{V}_F + \mathbf{I})^{-1} \mathbf{C}_w \tilde{\mathbf{A}}^* \tilde{\mathbf{A}} \right].$$

Recall that the goal of cOED problem is to minimize  $\tilde{\Psi}_{\text{f}}^{cA}$  over the design  $\mathbf{w}$ . Since  $\text{tr}(\mathbf{A} \mathbf{\Gamma}_{\text{pr}} \mathbf{A}^*)$  does not depend on  $\mathbf{w}$ , we can instead focus on minimizing

$$(5.7) \quad \tilde{\Psi}_{\text{f}-}^{cA} := - \text{tr} \left[ (\mathbf{C}_w \mathbf{V}_F^* \mathbf{V}_F + \mathbf{I})^{-1} \mathbf{C}_w \tilde{\mathbf{A}}^* \tilde{\mathbf{A}} \right].$$

Note that we have expressed the design criterion  $\tilde{\Psi}_{\text{f}-}^{cA}$  as the trace of a  $k_f$ -dimensional operator. The expression in (5.7) involving the trace can be computed efficiently with no further need for applications of  $\mathbf{F}$  and its adjoint. Furthermore, we may also precompute the operator

$\tilde{\mathbf{A}} = \mathbf{A}\mathbf{\Gamma}_{\text{pr}}^{1/2}\mathbf{V}_F$  by performing  $k_f$  applications of the goal operator  $\mathbf{A}$ . With the requisite pre-computations in place, all subsequent evaluations of  $\tilde{\Psi}_{f-}^{cA}$  can be performed with no need for further PDE solves. We summarize the steps for computing  $\tilde{\Psi}_{f-}^{cA}$  in [Procedure 1](#).

---

**Procedure 1** Frozen Low-Rank Evaluation of cOED Objective

---

*Offline*

Approximate  $\tilde{\mathbf{F}} \approx \mathbf{U}_F \mathbf{V}_F^*$  ▷ cost:  $\mathcal{O}(k_f)$  applies of  $\mathbf{F}$  and  $\mathbf{F}^*$

Precompute  $\tilde{\mathbf{A}} = \mathbf{A}\mathbf{\Gamma}_{\text{pr}}^{1/2}\mathbf{V}_F$  ▷ cost:  $k_f$  applications of goal operator  $\mathbf{A}$

Compute  $\tilde{\mathbf{A}}^* \tilde{\mathbf{A}}$  and  $\mathbf{V}_F^* \mathbf{V}_F$

*Online*

Compute  $\mathbf{C}_w = \mathbf{U}_F^\top \mathbf{W}_\sigma \mathbf{U}_F$  and evaluate (5.7)

---

Thus far, we have focused on computing the cOED criterion using the frozen low-rank forward operator approach. The spectral approach discussed in [Section 5.2.1](#) can be used to derive an approximate criterion analogous to (5.7). One important downside to the spectral approach is that the low-rank approximation of the prior-preconditioned data-misfit Hessian depends on the design  $\mathbf{w}$ . Therefore, for each evaluation of the cOED objective,  $\mathcal{O}(k_h)$  forward/adjoint PDE solves for the Hessian approximation are necessary. Note, however, that  $k_h$  is typically much smaller than the numerical rank  $k_f$  of  $\tilde{\mathbf{F}}$ , which was considered in the frozen low-rank approach. Namely,  $k_h$  is bounded by the number of active sensors in a design; i.e., for a given design  $\mathbf{w}$ ,  $k_h \leq \|\mathbf{w}\|_1$ . Given  $\mathbf{w}$ , we can compute  $\tilde{\mathbf{A}}_h = \mathbf{A}\mathbf{\Gamma}_{\text{pr}}^{1/2}\mathbf{V}$  to obtain the approximation,

$$\mathbf{A}\tilde{\mathbf{\Gamma}}_{\text{post,h}}\mathbf{A}^* = \mathbf{A}\mathbf{\Gamma}_{\text{pr}}\mathbf{A}^* - \tilde{\mathbf{A}}_h\mathbf{D}\tilde{\mathbf{A}}_h^*.$$

As before, we can ignore the design-invariant terms when optimizing the cOED criterion—we can instead focus on minimizing

$$\tilde{\Psi}_{h-}^{cA}(\mathbf{w}) := -\text{tr}(\tilde{\mathbf{A}}_h\mathbf{D}(\mathbf{w})\tilde{\mathbf{A}}_h^*).$$

We summarize the cost of the two approaches when using greedy optimization in terms of the number of PDE solves in [Table 2](#). Note that we exclude the cost associated with applying prior covariance operators, as they are often much smaller than the cost of applying  $\mathbf{A}$ ,  $\mathbf{F}$ , and their adjoints. It is notable, nevertheless, that the frozen approach does not require any online applications of the prior covariance operator either.

Method	Total Offline Cost	Total Online Cost
Spectral approach ( <a href="#">Section 5.2.1</a> )	—	$\mathcal{O}(k_h \cdot kn_s)$
Frozen approach ( <a href="#">Section 5.2.2</a> )	$\mathcal{O}(k_f)$	—

Table 2: Computational cost of the methods (in number of PDE solves)

To evaluate the entire expression for the cOED criterion  $\Psi^{cA}$ , with either approach, we need the design-invariant quantity  $\text{tr}(\mathbf{A}\mathbf{\Gamma}_{\text{pr}}\mathbf{A}^*)$ . Although not necessary for optimization,

efficient matrix-free evaluation of this quantity is needed for post-inference analysis (see [Section 5.3](#)). A similarity transform of  $\mathbf{A}\mathbf{\Gamma}_{\text{pr}}\mathbf{A}^*$  yields the symmetric, positive-definite matrix  $\mathbf{M}_u^{1/2}\mathbf{A}\mathbf{\Gamma}_{\text{pr}}\mathbf{A}^*\mathbf{M}_u^{-1/2}$ , which is convenient to work with. Since the trace is invariant under a similarity transformation, we focus on computing  $\text{tr}(\mathbf{M}_u^{1/2}\mathbf{A}\mathbf{\Gamma}_{\text{pr}}\mathbf{A}^*\mathbf{M}_u^{-1/2})$ . In this article, we employ the structure-exploiting XNYS TRACE algorithm proposed in [\[21\]](#) for the efficient estimation of this trace. Since this quantity is design-invariant, it only needs to be computed once.

**5.3. Efficient estimation of expectation and variance of  $\Phi_{\text{ctrl}}^*$ .** Here, we discuss fast computation of the posterior mean and variance of the control objective. Let us first consider  $\mathbb{E}(\Phi_{\text{ctrl}}^*|\mathbf{y})$ , which can be represented as [\(4.7\)](#). Note that computing this expected value requires the computation of the criterion  $\Psi^{cA}$ , the MAP estimate  $\mathbf{m}_{\text{MAP}}^{\mathbf{y}}$ , and the objective  $\Phi_{\text{ctrl}}^*(\mathbf{m}_{\text{MAP}}^{\mathbf{y}})$ . Of these quantities, the computational cost of estimating  $\mathbb{E}(\Phi_{\text{ctrl}}^*|\mathbf{y})$  is dominated by the estimation of the cOED criterion, for which efficient techniques are outlined in [Section 5.2](#).

We next consider the expression for the variance of the control objective from [\(4.6\)](#). The key challenge for computing this variance expression is computing the trace of  $(\mathbf{A}\mathbf{\Gamma}_{\text{post}}\mathbf{A}^*)^2$ . This trace can be estimated efficiently by utilizing the approximate posterior covariance  $\tilde{\mathbf{\Gamma}}_{\text{post},f}$ . In particular, note that

$$\begin{aligned} \text{tr}((\mathbf{A}\tilde{\mathbf{\Gamma}}_{\text{post},f}\mathbf{A}^*)^2) &= \text{tr}\left((\mathbf{A}\mathbf{\Gamma}_{\text{pr}}\mathbf{A}^* - \tilde{\mathbf{A}}(\mathbf{C}_w\mathbf{V}_F^*\mathbf{V}_F + \mathbf{I})^{-1}\mathbf{C}_w\tilde{\mathbf{A}}^*)^2\right) \\ &= \text{tr}((\mathbf{A}\mathbf{\Gamma}_{\text{pr}}\mathbf{A}^*)^2) + \text{tr}\left(((\mathbf{C}_w\mathbf{V}_F^*\mathbf{V}_F + \mathbf{I})^{-1}\mathbf{C}_w\tilde{\mathbf{A}}^*\tilde{\mathbf{A}})^2\right) \\ &\quad - 2\text{tr}\left((\mathbf{C}_w\mathbf{V}_F^*\mathbf{V}_F + \mathbf{I})^{-1}\mathbf{C}_w\mathbf{G}^*\mathbf{G}\right), \end{aligned}$$

where  $\mathbf{G} := \mathbf{\Gamma}_{\text{pr}}^{1/2}\mathbf{A}^*\tilde{\mathbf{A}}$ . We compute the design-independent additive quantities in the above expression in an offline efficient matrix-free manner similar to as described in the end of [Section 5.2](#). In fact, computations for estimating  $\text{tr}(\mathbf{A}\mathbf{\Gamma}_{\text{pr}}\mathbf{A}^*)$  can be reused for estimating  $\text{tr}((\mathbf{A}\mathbf{\Gamma}_{\text{pr}}\mathbf{A}^*)^2)$ . Specifically, we can reuse the randomized Nyström approximation of  $\mathbf{A}\mathbf{\Gamma}_{\text{pr}}\mathbf{A}^*$  computed in XNYS TRACE to obtain an approximation of  $(\mathbf{A}\mathbf{\Gamma}_{\text{pr}}\mathbf{A}^*)^2$ . The trace of this approximation can be used as an estimate to  $\text{tr}((\mathbf{A}\mathbf{\Gamma}_{\text{pr}}\mathbf{A}^*)^2)$ , avoiding additional PDE solves.

**6. Numerical results.** In this section, we present our numerical experiments pertaining to the cOED framework. The motivating example of a two-dimensional heat transfer application from [Section 2](#) is used as a testbed for the proposed approach. In [Sections 6.1](#) and [6.2](#), we describe the discretized inverse and optimal control problems for this model problem. We next study the low-rank approximation of the prior-preconditioned parameter-to-observable map and its use for fast computation of the cOED criterion in [Section 6.3](#). This analysis lays the groundwork for [Section 6.4](#), in which we solve the OED problem and demonstrate the effectiveness of cOED in comparison with classical approaches.

**6.1. Inverse problem.** Consider the problem of reconstructing the unknown source parameter  $m$  from sensor measurements of  $\hat{u}$  in [\(2.3\)](#). To discretize the problem, we employ linear triangular continuous Galerkin finite elements with  $N = L = 961$  degrees of freedom (a  $30 \times 30$  mesh), yielding discretized parameters  $\mathbf{m}$  and  $\hat{\mathbf{u}}$ . Following the approach in [\[14\]](#), we define a prior distribution  $\mu_{\text{pr}} = \mathcal{N}(\mathbf{0}, \mathbf{\Gamma}_{\text{pr}})$ , where the prior covariance operator is the

discretization of a squared inverse of an elliptic differential operator. In particular, we define  $\mathbf{\Gamma}_{\text{pr}}^{1/2} := (\alpha \mathbf{K} + \beta \mathbf{M})^{-1} \mathbf{M}$ , where  $\mathbf{M}$  and  $\mathbf{K}$  represent the finite-element mass and stiffness matrices, respectively. Here, we use  $\alpha = 0.1$  and  $\beta = 1$ . To provide some insight, we show the prior variance field in Figure 3.

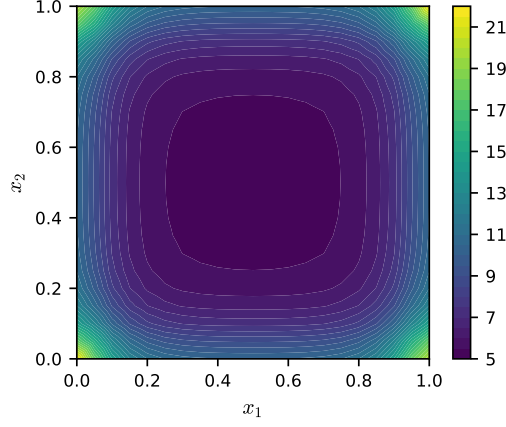


Figure 3: Prior pointwise variance field

To facilitate the numerical experiments that follow, we generate synthetic data by manufacturing a *ground-truth* inversion parameter,  $\mathbf{m}_{\text{true}}$ , as shown in Figure 4 (left). Using  $\mathbf{m}_{\text{true}}$ , we solve the forward model (2.3) to obtain sensor data  $\mathbf{y}$  on a uniform grid of  $n_y = 81$  candidate sensor locations, as visualized in Figure 4 (right). To emulate measurement noise, we add to this  $\mathbf{y}$  a random draw  $\boldsymbol{\eta} \sim \mathcal{N}(\mathbf{0}, \mathbf{\Gamma}_{\text{noise}})$ . Here, we use  $\mathbf{\Gamma}_{\text{noise}} = \sigma^2 \mathbf{I}_{n_y}$ , where  $\sigma := \frac{\delta}{\sqrt{n_y}} \|\mathbf{F} \mathbf{m}_{\text{true}} + \mathbf{b}\|_2$  with  $\delta = 0.01$ , resulting in a (normalized) noise level of 1%.

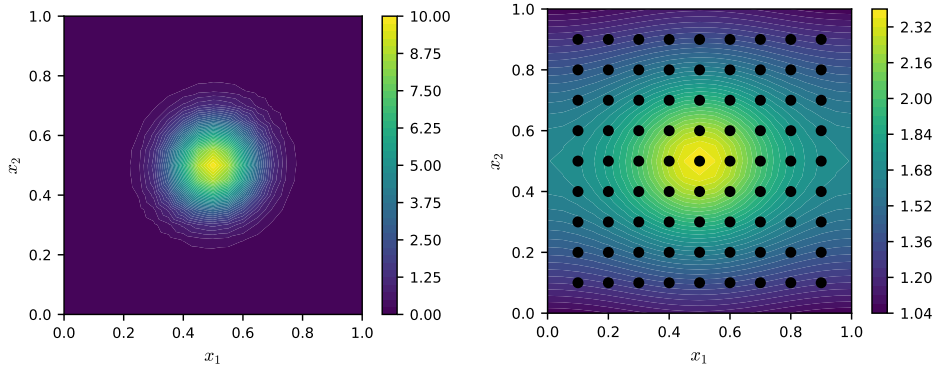


Figure 4: Ground-truth inversion parameter  $\mathbf{m}_{\text{true}}$  (left) and initial condition  $\hat{\mathbf{u}}$  (right).

We solve the inverse problem using synthetic measurement data obtained at all candidate sensor locations, and in Figure 5, we plot the resulting posterior mean  $\mathbf{m}_{\text{MAP}}$  and the pointwise

posterior variance field.

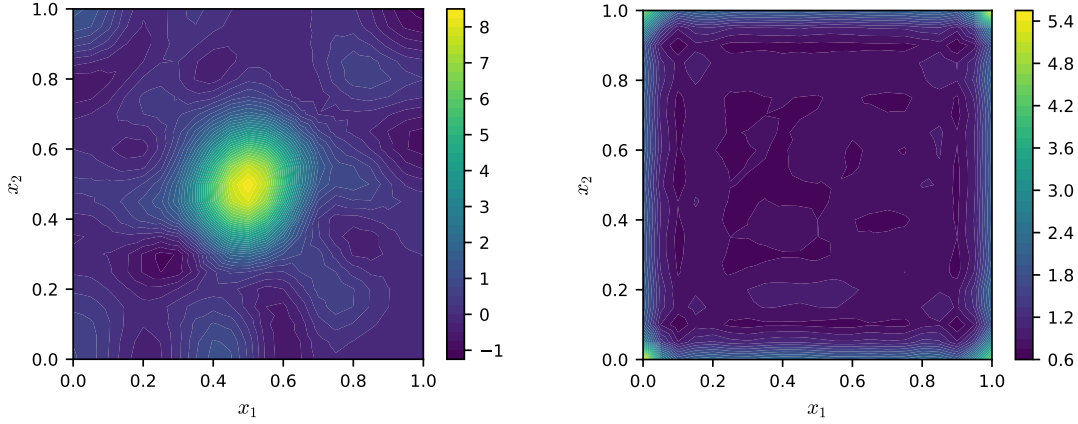


Figure 5: Posterior mean  $\mathbf{m}_{\text{MAP}}$  (left) and pointwise variance (right).

**6.2. The optimal control problem.** Let us revisit the optimal control problem pertaining to the motivating application in Section 2. We would like to solve for an optimal control that guides the transient advection-diffusion model towards a target state by controlling the intensity of a heat source. Here, we consider a uniform target state,  $\bar{\mathbf{u}} \equiv 1$  and the velocity field  $\mathbf{v}(\mathbf{x}) := [-x_2 - 0.5 x_1 - 0.5]^\top$ . This solenoidal velocity field corresponds to a counterclockwise circular field around the center,  $(x_1, x_2) = (0.5, 0.5)$ . We consider a time interval  $[0, 1]$  discretized by  $K = 20$  evenly spaced time steps. The forward and adjoint PDEs are solved using backward Euler time stepping. In addition, to integrate spatio-temporal quantities, we utilize a temporal mass matrix  $\mathbf{M}_z$  based on the composite midpoint rule.

Given this setup, we solve the optimization problem (3.10) with regularization parameter  $\beta := 10^{-5}$  to obtain a nominal control estimate,  $\mathbf{z}^*$ , corresponding to  $\mathbf{m}_{\text{MAP}}$ . The resulting control and terminal state are shown in Figure 6. The nominal control yields a (non-regularized) control objective of  $\Phi_{\text{ctrl}}^*(\mathbf{m}_{\text{true}}) = 0.039$ , yielding a terminal state that is 83% closer to the target state compared to the initial state.

**6.3. Spectral analysis of prior-preconditioned forward operator.** In this section, we study the spectral decay of the prior-preconditioned forward operator. This provides insight regarding the accuracy of the frozen low-rank approximation technique in the computation of the cOED criterion and the uncertainty measures in Section 5.

Figure 7 (left) shows rapid decay of the singular values corresponding to the prior-preconditioned forward operator. Recall that the rank of  $\tilde{\mathbf{F}}$  is limited by the dimension of candidate sensors, which is already typically much smaller than the discretized parameter dimension. Furthermore, the spectral decay of this operator observed here validates that an even lower-rank approximation can capture the dominant features of the operator.

In addition to visualizing the spectral decay of  $\tilde{\mathbf{F}}$ , we analyze the impact of rank- $k_f$  truncation on the accuracy of the estimated cOED criterion in Figure 7 (right). This is analyzed

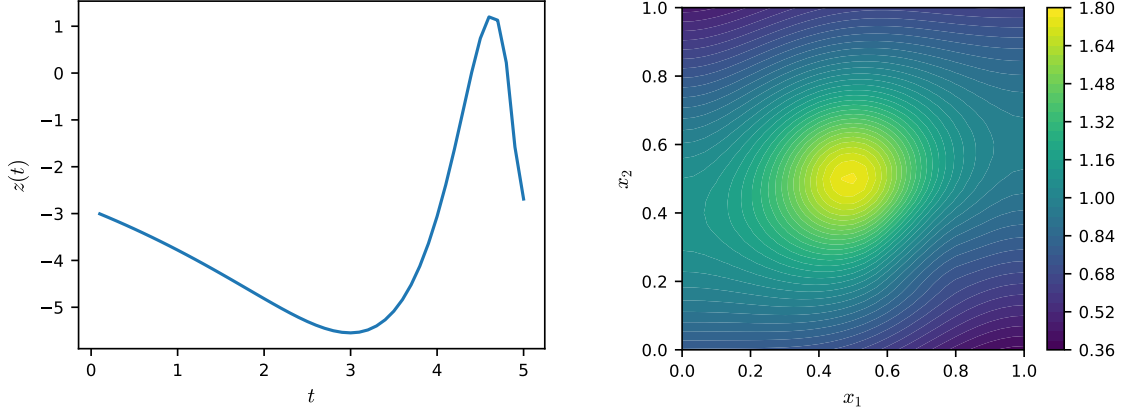


Figure 6: Nominal control  $\mathbf{z}^*$  (left) and terminal state  $\mathbf{u}_T(\mathbf{m}_{\text{MAP}}, \mathbf{z}^*)$  (right).

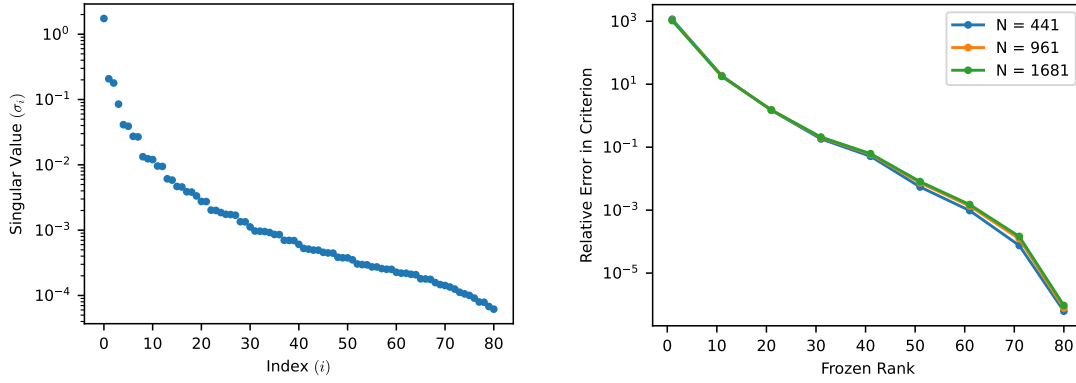


Figure 7: Singular values of  $\tilde{\mathbf{F}}$  (left) and relative error of  $\Psi^{cA}$  over  $k_f$  (right).

by computing the relative error of the estimated cOED criterion using [Procedure 1](#) with the cOED criterion computing the exact posterior. We observe a near-exponential decay of the error, which reinforces that modest low-rank approximations can produce accurate estimates of the criterion. In [Figure 7](#) (right), we also plot the relative error of  $\Psi^{cA}$  across different mesh resolutions. The results show consistent criterion estimates across all resolutions.

**6.4. Optimal experimental design.** In this section, we investigate classical and cOED techniques and demonstrate the effectiveness of the control-oriented approach.

**6.4.1. Solving the OED Problem.** We consider a fixed budget of  $k = 13$  sensors. In the experiments that follow, we use the greedy approach from [Algorithm 5.1](#) to select 13 sensor locations out of the candidate sensors depicted in [Figure 4](#) (right) that minimize a specified design criteria. For fast evaluations of the criteria in each iteration, we utilize the frozen low-rank approximation approach from [Section 5](#) (see [Procedure 1](#)). The resulting classical

A-optimal and control-oriented optimal designs are displayed in Figure 8.

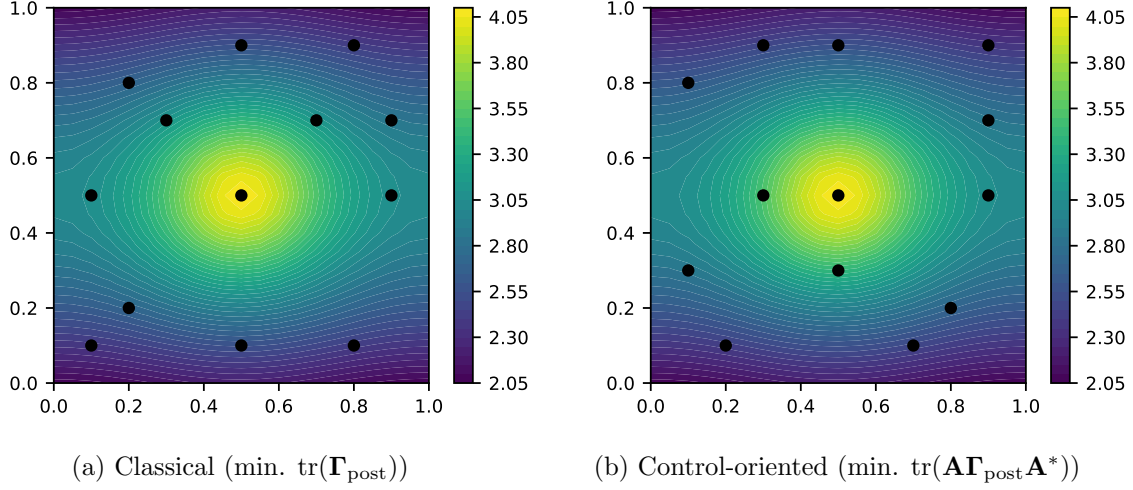


Figure 8: Optimal experimental designs for the heat transfer problem.

Recall that the classical A-optimal criterion minimizes average posterior variance of the inversion parameter. On the other hand, as discussed in Section 4, the control-oriented approach instead seeks a reconstruction that minimizes uncertainty in the terminal state. In Table 3, we compare the measures of posterior uncertainty induced by utilizing classical and control-oriented optimal designs. The reported results demonstrate that the control-oriented optimal placement of sensors can yield significant benefits over classical approaches. In particular, we observe that when using cOED, the average posterior variance of the terminal state is 19% smaller than that obtained using a classical A-optimal sensor placement.

Design	$\text{tr}[\mathbf{\Gamma}_{\text{post}}]$	$\text{tr}[\mathbf{A}\mathbf{\Gamma}_{\text{post}}\mathbf{A}^*]$
Classical	<b>0.590</b>	$2.26 \times 10^{-3}$
Control-oriented	0.616	<b><math>1.83 \times 10^{-3}</math></b>

Table 3: Comparison of classical A-optimal and control-oriented sensor placements.

It is also informative to consider the optimized designs against random sensor selections. To this end, we generate a sample of 1000 random sensor placements with the same number of sensors and compare them to the optimized designs; see Figure 9. Note that although there are combinatorially many possible design choices, these random sensor placements serve as a feasible and representative sample for comparison. The results demonstrate that both classical and control-oriented designs outperform nearly all random designs. Furthermore,

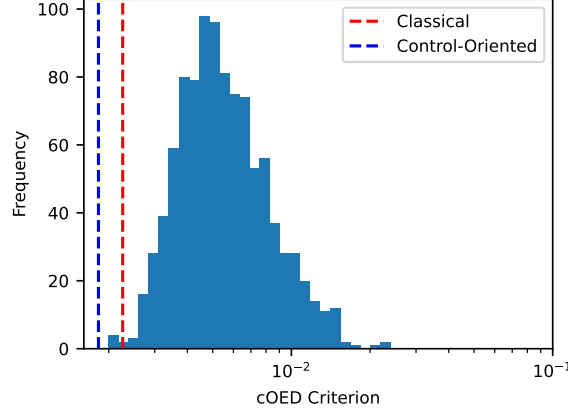
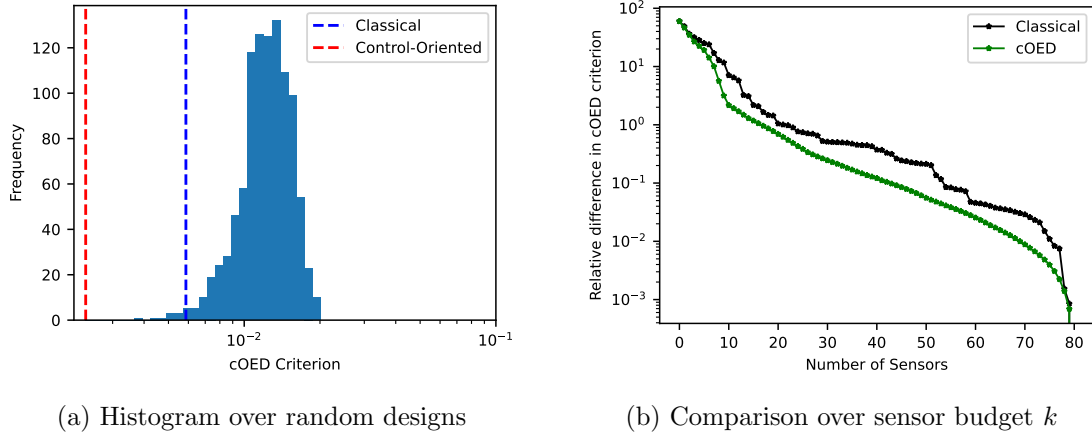


Figure 9: Comparison of cOED criterion for random, classical and control-oriented designs.

as noted previously, we observe that the control-oriented design outperforms the classical A-optimal design. It is worth highlighting that the benefit of cOED can be much larger in many practical applications. For example, applying cOED to even the same control problem studied here but equipped with a slightly stronger advection field can yield much larger (e.g.,  $> 50\%$ ) improvement in the cOED criterion compared to a classical A-optimal design. As seen in Figure 10a, we observe roughly 60% improvement when the advection field  $\mathbf{v}(\mathbf{x})$  is scaled by a factor of five. Moreover, the performance also varies depending on the sensor budget  $k$  chosen. To analyze the effect of the sensor budget, we compare the cOED criterion evaluated at the control-oriented and classical designs for varying sensor budgets in Figure 10b. For better visualization, we display the relative difference of the cOED criterion with sensor budget  $k$  to the criterion evaluated with all candidate sensors active.



(a) Histogram over random designs

(b) Comparison over sensor budget  $k$

Figure 10: Comparison of cOED, classical, and random designs (scaled advection).

**6.4.2. Control-Oriented Uncertainty Quantification.** Here, we further study the effectiveness of control-oriented sensor placements in reducing the uncertainty in the terminal state. In Figure 11a, we report the pointwise posterior variance field of the terminal state; this is compared with an evenly-spaced sensor placement Figure 11b, as well as two random designs with an equivalent number of sensors Figures 11c and 11d. With both random and evenly-spaced sensor placements, we observe elevated amounts of posterior uncertainty in parts of the domain compared to cOED. The results indicate a significant reduction in the posterior uncertainty with the control-oriented approach.

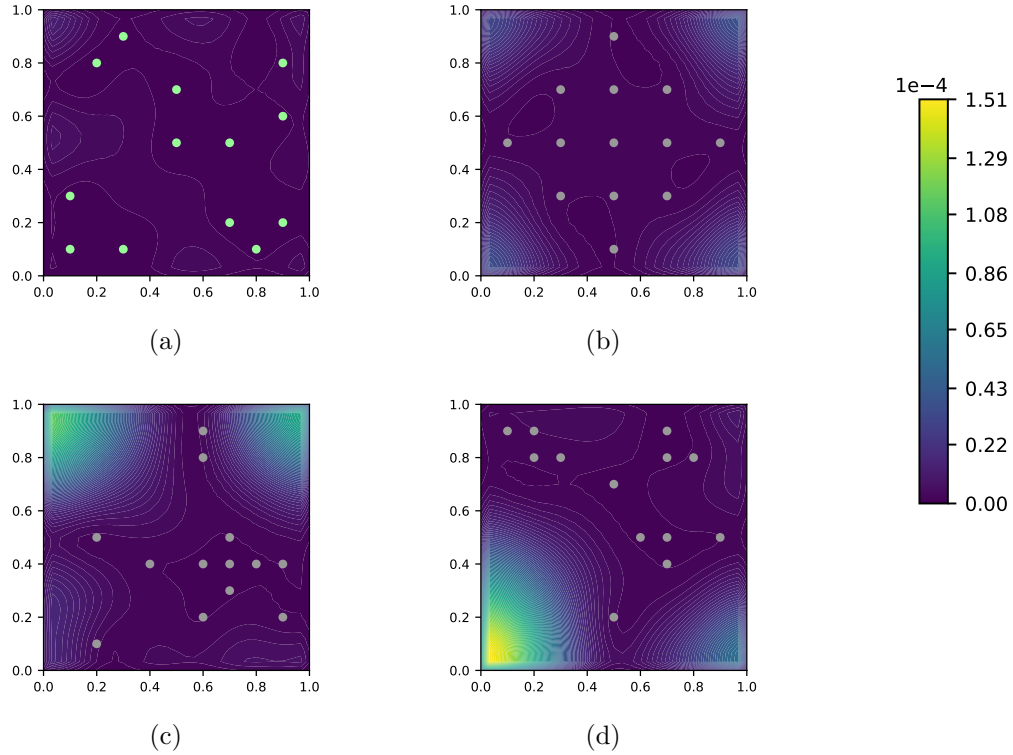


Figure 11: Posterior uncertainty in  $u_T$  with cOED (a), evenly-spaced designs (b), and random designs (c-d).

We next consider the expectation and variance of the control objective with respect to the posterior; see Section 4.2. It is important to note that these posterior quantities rely on data and therefore must be interpreted with caution. In light of this, we consider a reachable target state  $\bar{u}$  in the experiments that follow. Nevertheless, in the present experiment, cOED provides an expected control objective and a variance that is significantly better than almost all evaluated random designs as seen in Figure 12. This suggests that cOED can potentially be effective at aiding reduction of the control objective, as well as reduced uncertainty in the control objective. This is in line with our theoretical observations in Section 4.2.

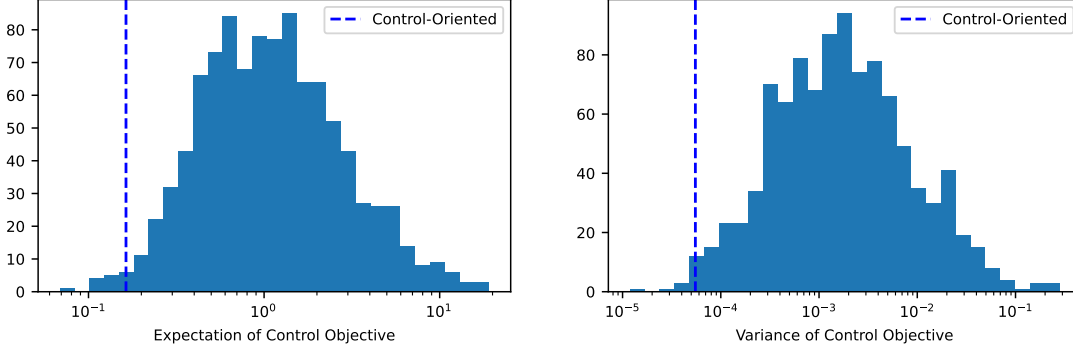


Figure 12:  $\mathbb{E}(\Phi_{\text{ctrl}}^* | \mathbf{y})$  (left) and  $\text{Var}(\Phi_{\text{ctrl}}^* | \mathbf{y})$  (right) obtained using the control-oriented design as well as random designs.

**7. Conclusions.** In this article, we have developed a mathematical and computational framework for control-oriented optimal sensor placement. The focus is on problems involving control of linear PDEs with linear dependence on inversion parameters. The proposed approach takes the coupling of the optimal control problem and the associated inverse problem into account to derive a control-oriented experimental design criterion. This framework also enables quantifying the uncertainty in the control objective. The proposed mathematical framework is complemented by scalable computational methods for solving the control-oriented OED (cOED) problem and quantifying the uncertainty in the terminal state and the control objective. In particular, at the up-front cost of a modest number of PDE solves, the proposed frozen low-rank forward operator approach enables solving the cOED problem with no need for solving the PDEs governing the inverse and optimal control problems, within the optimization loop.

Our numerical results demonstrate the effectiveness of the proposed strategy and the importance of the control-oriented approach. Specifically, the control-oriented optimal sensor placements outperform classical A-optimal sensor placements in terms of reducing the posterior uncertainty in the terminal state in the PDEs governing the optimal control problem. Additionally, the posterior distribution obtained using the control-oriented optimal sensor placements provide near-optimal uncertainty reduction in the control objective.

There are several interesting avenues for further investigations. In the first place, one can consider sensor placement for the cases where the optimal control problem has nonlinear dependence on the inversion parameters or the cases where the associated inverse problem is nonlinear. For example, in the case of nonlinear inverse problems, a Laplace approximation to the posterior provides a first step in deriving approximate control-oriented measures of posterior uncertainty that are tractable to optimize. To provide more accurate estimates of control-oriented measures of posterior uncertainty, sampling-based approaches are needed. To make such sampling approaches tractable, derivative-informed surrogate-based approaches considered in [16, 26, 48] provide attractive options. Another interesting area for further investigation is to consider alternative approaches for defining a control-oriented criterion. These

include a control-oriented D-optimality criterion, defined similarly to the goal-oriented setting in [10], or a risk-adapted approach such as the one in [42].

**Acknowledgments.** This article has been authored by employees of National Technology & Engineering Solutions of Sandia, LLC under Contract No. DE-NA0003525 with the U.S. Department of Energy (DOE). The employees own all right, title and interest in and to the article and are solely responsible for its contents. The United States Government retains and the publisher, by accepting the article for publication, acknowledges that the United States Government retains a non-exclusive, paid-up, irrevocable, worldwide license to publish or reproduce the published form of this article or allow others to do so, for United States Government purposes. The DOE will provide public access to these results of federally sponsored research in accordance with the DOE Public Access Plan <https://www.energy.gov/downloads/doe-public-access-plan>. This paper describes objective technical results and analysis. Any subjective views or opinions that might be expressed in the paper do not necessarily represent the views of the U.S. Department of Energy or the United States Government. SAND2025-019030.

## REFERENCES

- [1] V. AKÇELİK, G. BIROS, A. DRĂGĂNESCU, O. GHATTAS, J. HILL, AND B. VAN BLOEMAN WAANDERS, *Dynamic data-driven inversion for terascale simulations: Real-time identification of airborne contaminants*, in Proceedings of SC2005, 2005.
- [2] A. ALEXANDERIAN, *Optimal experimental design for infinite-dimensional Bayesian inverse problems governed by PDEs: A review*, Inverse Problems, 37 (2021), p. 043001.
- [3] A. ALEXANDERIAN, N. PETRA, G. STADLER, AND O. GHATTAS, *A-optimal design of experiments for infinite-dimensional Bayesian linear inverse problems with regularized  $\ell_0$ -sparsification*, SIAM Journal on Scientific Computing, 36 (2013).
- [4] A. ALEXANDERIAN, N. PETRA, G. STADLER, AND O. GHATTAS, *A-optimal design of experiments for infinite-dimensional bayesian linear inverse problems with regularized  $\ell_0$ -sparsification*, SIAM Journal on Scientific Computing, 36 (2014), pp. A2122–A2148.
- [5] A. ALEXANDERIAN, N. PETRA, G. STADLER, AND O. GHATTAS, *Mean-variance risk-averse optimal control of systems governed by pdes with random parameter fields using quadratic approximations*, SIAM/ASA Journal on Uncertainty Quantification, 5 (2017), pp. 1166–1192.
- [6] A. ALEXANDERIAN AND A. K. SAIBABA, *Efficient D-optimal design of experiments for infinite dimensional Bayesian linear inverse problems*, SIAM Journal on Scientific Computing, 40 (2017), pp. A2956–A2985.
- [7] A. ALEXANDERIAN AND A. K. SAIBABA, *Efficient d-optimal design of experiments for infinite-dimensional bayesian linear inverse problems*, SIAM Journal on Scientific Computing, 40 (2018), pp. A2956–A2985.
- [8] A. C. ATKINSON AND A. N. DONEV, *Optimum Experimental Designs*, Oxford, 1992.
- [9] A. ATTIA, A. ALEXANDERIAN, AND A. K. SAIBABA, *Goal-oriented optimal design of experiments for large-scale Bayesian linear inverse problems*, Inverse Problems, 34 (2018), p. 095009.
- [10] A. ATTIA, S. LEYFFER, AND T. S. MUNSON, *Stochastic learning approach to binary optimization for optimal design of experiments*, SIAM Journal on Scientific Computing, 44 (2021), pp. 395–.
- [11] D. S. BERNSTEIN, *Matrix Mathematics: Theory, Facts, and Formulas*, Princeton University Press, second ed., 2011.
- [12] A. A. BIAN, J. M. BUHMANN, A. KRAUSE, AND S. TSCHIATSCHEK, *Guarantees for greedy maximization of non-submodular functions with applications*, in International conference on machine learning, Proceedings of Machine Learning Research, 2017, pp. 498–507.
- [13] A. BORZÌ, V. SCHULZ, C. SCHILLINGS, AND G. VON WINCKEL, *On the treatment of distributed uncertainties in PDE-constrained optimization*, GAMM-Mitteilungen, 33 (2010), pp. 230–246.

- [14] T. BUI-THANH, O. GHATTAS, J. MARTIN, AND G. STADLER, *A computational framework for infinite-dimensional Bayesian inverse problems part I: The linearized case, with application to global seismic inversion*, SIAM Journal on Scientific Computing, 35 (2013), pp. A2494–A2523.
- [15] T. BUTLER, J. D. JAKEMAN, AND T. WILDEY, *Optimal experimental design for prediction based on push-forward probability measures*, Journal of Computational Physics, 416 (2020), p. 109518.
- [16] L. CAO, T. O’LEARY-ROSEBERRY, AND O. GHATTAS, *Efficient geometric Markov chain Monte Carlo for nonlinear Bayesian inversion enabled by derivative-informed neural operators*, arXiv preprint arXiv:2403.08220, (2024).
- [17] K. CHALONER AND I. VERDINELLI, *Bayesian experimental design: A review*, Statistical Science, 10 (1995), pp. 273–304.
- [18] P. CHEN AND O. GHATTAS, *Taylor approximation for chance constrained optimization problems governed by partial differential equations with high-dimensional random parameters*, SIAM/ASA Journal on Uncertainty Quantification, 9 (2021), pp. 1381–1410.
- [19] H. CHERNOFF, *A measure of asymptotic efficiency for tests of a hypothesis based on the sum of observations*, The Annals of Mathematical Statistics, 23 (1952), pp. 493–507.
- [20] A. CORTINOVIS AND D. KRESSNER, *On randomized trace estimates for indefinite matrices with an application to determinants*, Foundations of Computational Mathematics, 22 (2022), pp. 875–903.
- [21] E. N. EPPERLY, J. A. TROPP, AND R. J. WEBBER, *Xtrace: Making the most of every sample in stochastic trace estimation*, SIAM Journal on Matrix Analysis and Applications, 45 (2024), pp. 1–23, <https://doi.org/10.1137/23M1548323>.
- [22] H. P. FLATH, L. C. WILCOX, V. AKÇELİK, J. HILL, B. VAN BLOEMEN WAANDERS, AND O. GHATTAS, *Fast algorithms for Bayesian uncertainty quantification in large-scale linear inverse problems based on low-rank partial hessian approximations*, SIAM Journal on Scientific Computing, 33 (2011), pp. 407–432.
- [23] M. GEVERS, *Identification for control: From the early achievements to the revival of experiment design*, European Journal of Control, 11 (2005), pp. 335–352, <https://doi.org/10.3166/ejc.11.335-352>, <https://www.sciencedirect.com/science/article/pii/S0947358005710414>.
- [24] C. GIRAUD, *Introduction to High-Dimensional Statistics*, Chapman and Hall/CRC, New York, Dec. 2014, <https://doi.org/10.1201/b17895>.
- [25] A. GITTENS AND M. W. MAHONEY, *Revisiting the Nyström method for improved large-scale machine learning*, Journal of Machine Learning Research, 17 (2013), pp. 117:1–117:65.
- [26] J. GO AND P. CHEN, *Accelerating Bayesian optimal experimental design with derivative-informed neural operators*, arXiv preprint arXiv:2312.14810, (2024).
- [27] M. D. GUNZBURGER, *Perspectives in Flow Control and Optimization*, Society for Industrial and Applied Mathematics, 2002, <https://doi.org/10.1137/1.9780898718720>.
- [28] M. D. GUNZBURGER AND J. MING, *Optimal control of stochastic flow over a backward-facing step using reduced-order modeling*, SIAM Journal on Scientific Computing, 33 (2011), pp. 2641–2663, <https://doi.org/10.1137/100817279>, <http://link.aip.org/link/?SCE/33/2641/1>.
- [29] W. W. HAGER, *Updating the inverse of a matrix*, SIAM Review, 31 (1989), pp. 221–239.
- [30] N. HALKO, P. G. MARTINSSON, AND J. A. TROPP, *Finding structure with randomness: Probabilistic algorithms for constructing approximate matrix decompositions*, SIAM Review, 53 (2009), pp. 217–288.
- [31] D. L. HANSON AND F. T. WRIGHT, *A bound on tail probabilities for quadratic forms in independent random variables*, The Annals of Mathematical Statistics, 42 (1971), pp. 1079–1083.
- [32] R. HARMAN, L. FILOVÁ, AND P. RICHTÁRIK, *A randomized exchange algorithm for computing optimal approximate designs of experiments*, Journal of the American Statistical Association, 115 (2018), pp. 348 – 361.
- [33] R. HERZOG, I. RIEDEL, AND D. UCIŃSKI, *Optimal sensor placement for joint parameter and state estimation problems in large-scale dynamical systems with applications to thermo-mechanics*, Optimization and Engineering, 19 (2018), pp. 591–627.
- [34] H. HJALMARSSON, *From experiment design to closed-loop control*, Automatica, 41 (2005), pp. 393–438, <https://doi.org/10.1016/j.automatica.2004.11.021>, <https://www.sciencedirect.com/science/article/pii/S0005109804003346>.
- [35] H. HMEDE, S. NICAISE, L. PAQUET, AND A. WEHBE, *Optimal control of the temperature by the laser path*

- and the thermal treatment time in selective laser melting process, *Mathematical Control and Related Fields*, (2024), <https://doi.org/10.3934/mcrf.2024025>.
- [36] X. HUAN, J. JAGALUR, AND Y. MARZOUK, *Optimal experimental design: Formulations and computations*, *Acta Numerica*, 33 (2024), pp. 715–840.
  - [37] J. P. IMHOF, *Computing the distribution of quadratic forms in normal variables*, *Biometrika*, 48 (1961), pp. 419–426.
  - [38] J. JAGALUR-MOHAN AND Y. MARZOUK, *Batch greedy maximization of non-submodular functions: Guarantees and applications to experimental design*, *Journal of Machine Learning Research*, 22 (2021), pp. 1–62.
  - [39] C. KESSEL, M. A. FIRESTONE, AND R. W. CONN, *Linear optimal control of tokamak fusion devices*, *Fusion Technology*, 17 (1990), pp. 391–411.
  - [40] K.-T. KIM, U. VILLA, M. PARNO, Y. MARZOUK, O. GHATTAS, AND N. PETRA, *hippylib-mug: A bayesian inference software framework for integration of data with complex predictive models under uncertainty*, *ACM Transactions on Mathematical Software*, 49 (2023), pp. 1–31.
  - [41] D. P. KOURI, M. HEINKENSCHLOSS, D. RIDZAL, AND B. G. VAN BLOEMEN WAANDERS, *A trust-region algorithm with adaptive stochastic collocation for PDE optimization under uncertainty*, *SIAM Journal on Scientific Computing*, 35 (2013), pp. A1847–A1879.
  - [42] D. P. KOURI, J. D. JAKEMAN, AND J. GABRIEL HUERTA, *Risk-adapted optimal experimental design*, *SIAM/ASA Journal on Uncertainty Quantification*, 10 (2022), pp. 687–716.
  - [43] C. LANCZOS, *An iteration method for the solution of the eigenvalue problem of linear differential and integral operators*, *Journal of research of the National Bureau of Standards*, 45 (1950), pp. 255–282, <https://doi.org/10.6028/JRES.045.026>.
  - [44] F. LI, *A combinatorial approach to goal-oriented optimal Bayesian experimental design*, master’s thesis, Massachusetts Institute of Technology, 2019.
  - [45] A. M. MATHAI AND S. B. PROVOST, *Quadratic Forms in Random Variables: Theory and Applications*, Marcel Dekker, New York, NY, 1992.
  - [46] K. MOSHKARSAR, *On the absolute constant in Hanson-Wright inequality*, 2024, <https://arxiv.org/abs/2111.00557>.
  - [47] K. MOSHKARSAR, *Refining concentration for gaussian quadratic chaos*, Jan. 2025, <https://doi.org/10.48550/arXiv.2412.03774>, <http://arxiv.org/abs/2412.03774> (accessed 2025-08-14). arXiv:2412.03774 [math].
  - [48] T. O’LEARY-ROSEBERRY, P. CHEN, U. VILLA, AND O. GHATTAS, *Derivative-informed neural operator: an efficient framework for high-dimensional parametric derivative learning*, *Journal of Computational Physics*, 496 (2024), p. 112555.
  - [49] N. PETRA AND G. STADLER, *Model variational inverse problems governed by partial differential equations*, Tech. Report 11-05, The Institute for Computational Engineering and Sciences, The University of Texas at Austin, 2011.
  - [50] L. PRONZATO, *Optimal experimental design and some related control problems*, *Automatica*, 44 (2008), pp. 303–325, <https://doi.org/https://doi.org/10.1016/j.automatica.2007.05.016>, <https://www.sciencedirect.com/science/article/pii/S0005109807002853>.
  - [51] F. PUKELSHEIM, *Optimal Design of Experiments*, Society for Industrial and Applied Mathematics, 2006, <https://doi.org/10.1137/1.9780898719109>.
  - [52] M. RUDELSON AND R. VERSHYNIN, *Hanson-wright inequality and sub-gaussian concentration*, *Electronic Communications in Probability*, 18 (2013), pp. 1–9.
  - [53] A. K. SAIBABA, J. HART, AND B. VAN BLOEMEN WAANDERS, *Randomized algorithms for generalized singular value decomposition with application to sensitivity analysis*, *Numerical Linear Algebra with Applications*, 28 (2021), p. e2364.
  - [54] A. SPANTINI, T. CUI, K. WILLCOX, L. TENORIO, AND Y. MARZOUK, *Goal-oriented optimal approximations of Bayesian linear inverse problems*, *SIAM Journal on Scientific Computing*, 39 (2017), pp. S167–S196, <https://doi.org/10.1137/16M1082123>, <https://doi.org/10.1137/16M1082123>.
  - [55] A. M. STUART, *Inverse problems: A Bayesian perspective*, *Acta Numerica*, 19 (2010), pp. 451–559.
  - [56] A. TARANTOLA, *Inverse Problem Theory and Methods for Model Parameter Estimation*, SIAM, Philadelphia, PA, 2005.
  - [57] L. TENORIO, *An introduction to data analysis and uncertainty quantification for inverse problems*, SIAM, 2017.

- [58] H. TIESLER, R. M. KIRBY, D. XIU, AND T. PREUSSER, *Stochastic collocation for optimal control problems with stochastic pde constraints*, SIAM Journal on Control and Optimization, 50 (2012), pp. 2659–2682.
- [59] F. TRÖLTZSCH, *Optimal control of partial differential equations: Theory, methods and applications*, Graduate studies in mathematics, Providence, R.I., 2010.
- [60] D. UCINSKI, *Optimal measurement methods for distributed parameter system identification*, CRC Press, Boca Raton, 2005.
- [61] K. WU, P. CHEN, AND O. GHATTAS, *An offline-online decomposition method for efficient linear Bayesian goal-oriented optimal experimental design: Application to optimal sensor placement*, SIAM Journal on Scientific Computing, 45 (2023), pp. B57–B77.
- [62] S. ZHONG, W. SHEN, T. CATANACH, AND X. HUAN, *Goal-oriented Bayesian optimal experimental design for nonlinear models using Markov chain Monte Carlo*, arXiv preprint arXiv:2403.18072, (2024).

**Appendix A. Discretization of the target state and control variables.** The discretization of the target state  $u_T \in \mathcal{U}$  can be performed similarly to the case of the inversion parameter, using a finite element approach. On the other hand, the discretization of the control variable  $z$  is problem dependent. Consider, for example, the case where the control is a function of time only, as is the case in the example in Section 2. In that case, the discretized control variable  $\mathbf{z}$  is obtained by considering its values at a set of time steps  $\{t_1, \dots, t_K\}$  in which case,  $\mathbf{z} = [z(t_1) \ z(t_2) \ \dots \ z(t_K)]^\top$ . The inner product corresponding to the discretization of the space  $\mathcal{Z}$  of controls is obtained similarly to the case of the inversion parameter described above. In the case where  $\mathcal{Z} = L^2(0, T)$ , the inner product of elements in  $\mathcal{Z}$  can be approximated using a quadrature rule with nodes at the time steps and takes the form  $\langle \mathbf{z}_1, \mathbf{z}_2 \rangle_{\mathbf{M}_z} := \mathbf{z}_1^\top \mathbf{M}_z \mathbf{z}_2$ , for  $\mathbf{z}_1$  and  $\mathbf{z}_2$  in  $\mathbb{R}^K$ . In this case,  $\mathbf{M}_z$  is a diagonal matrix with quadrature weights on its diagonal. The discretized control space is  $\mathbb{R}^K$  equipped with the inner product  $\langle \cdot, \cdot \rangle_{\mathbf{M}_z}$ . While the present definition concerns the case where  $\mathcal{Z} = L^2(0, T)$ , the finite-dimensional inner product space of the discretized control variable takes a similar form in general.

## Appendix B. Proofs.

**B.1. Proof of Proposition 4.1.** We first derive the expression for the first and second moments of a quadratic functional of a Gaussian random vector.

**Lemma B.1.** *Consider a multivariate normal random vector,  $\mathbf{x} \sim \mathcal{N}(\boldsymbol{\mu}, \boldsymbol{\Sigma})$ , where  $\boldsymbol{\mu} \in \mathbb{R}^n$  and  $\boldsymbol{\Sigma} \in \mathbb{R}^{n \times n}$  is symmetric positive-definite (SPD). Let  $\mathbf{N}$  be an SPD matrix. Then the quadratic form,*

$$(B.1) \quad Q(\mathbf{x}) = \langle \mathbf{x}, \mathbf{N}\mathbf{x} \rangle = \|\mathbf{x}\|_{\mathbf{N}}^2,$$

has

$$(B.2a) \quad \mathbb{E} \{Q(\mathbf{x})\} = \text{tr}(\mathbf{N}\boldsymbol{\Sigma}) + \boldsymbol{\mu}^\top \mathbf{N}\boldsymbol{\mu},$$

$$(B.2b) \quad \text{Var} \{Q(\mathbf{x})\} = 2 \text{tr} [(\mathbf{N}\boldsymbol{\Sigma})^2] + 4\boldsymbol{\mu}^\top \mathbf{N}\boldsymbol{\Sigma}\mathbf{N}\boldsymbol{\mu}.$$

*Proof.* Let  $\hat{\mathbf{z}} := \boldsymbol{\Sigma}^{-1/2}(\mathbf{x} - \boldsymbol{\mu})$  be the standardized form of  $\mathbf{x}$ . One can express  $\mathbf{x}$  in terms of  $\hat{\mathbf{z}}$  as  $\mathbf{x} = \boldsymbol{\Sigma}^{1/2}(\hat{\mathbf{z}} + \boldsymbol{\Sigma}^{-1/2}\boldsymbol{\mu})$ . Consider the spectral decomposition,  $\boldsymbol{\Sigma}^{1/2}\mathbf{N}\boldsymbol{\Sigma}^{1/2} = \mathbf{U}\boldsymbol{\Lambda}\mathbf{U}^\top$ .

Then,

$$\begin{aligned} Q(\mathbf{x}) &= \mathbf{x}^\top \mathbf{N} \mathbf{x} = (\hat{\mathbf{z}} + \Sigma^{-1/2} \boldsymbol{\mu})^\top \Sigma^{1/2} \mathbf{N} \Sigma^{1/2} (\hat{\mathbf{z}} + \Sigma^{-1/2} \boldsymbol{\mu}) \\ &= (\hat{\mathbf{z}} + \Sigma^{-1/2} \boldsymbol{\mu})^\top \mathbf{U} \mathbf{\Lambda} \mathbf{U}^\top (\hat{\mathbf{z}} + \Sigma^{-1/2} \boldsymbol{\mu}) \\ &= (\mathbf{U}^\top \hat{\mathbf{z}} + \mathbf{U}^\top \Sigma^{-1/2} \boldsymbol{\mu})^\top \mathbf{\Lambda} (\mathbf{U}^\top \hat{\mathbf{z}} + \mathbf{U}^\top \Sigma^{-1/2} \boldsymbol{\mu}). \end{aligned}$$

For convenience, denote  $\mathbf{z} := \mathbf{U}^\top \hat{\mathbf{z}}$ , and  $\mathbf{b} := \mathbf{U}^\top \Sigma^{-1/2} \boldsymbol{\mu}$ . Then,

$$(B.3) \quad Q(\mathbf{x}) = (\mathbf{z} + \mathbf{b})^\top \mathbf{\Lambda} (\mathbf{z} + \mathbf{b}) = \sum_{i=1}^n \lambda_i (z_i + b_i)^2.$$

Thus, the quadratic term follows a generalized chi-squared distribution,

$$Q(\mathbf{x}) \sim \tilde{\chi}^2(\{\lambda_i\}_1^n, \{d_i\}_1^n, \{b_i^2\}_1^n, 0, 0)$$

where  $d_i$  denotes the multiplicity of the  $i$ -th eigenvalue. Here, it is important to note that  $z_i \sim \mathcal{N}(0, 1)$  are independent standard normal random variables. This form can be used to obtain the mean and variance of  $Q(\mathbf{x})$  as in (B.5). These expressions are straightforward to derive (based on linearity) and we refer to [37] and [45] for an in-depth discussion of generalized chi-squared random variables:

$$(B.4) \quad \mathbb{E}\{Q(\mathbf{x})\} = \sum_{i=1}^n \lambda_i (1 + b_i^2) = \text{tr}(\mathbf{N} \Sigma) + \boldsymbol{\mu}^\top \mathbf{N} \boldsymbol{\mu},$$

$$(B.5) \quad \text{Var}\{Q(\mathbf{x})\} = 2 \sum_{i=1}^n \lambda_i^2 (1 + 2b_i^2) = 2 \text{tr}[(\mathbf{N} \Sigma)^2] + 4 \boldsymbol{\mu}^\top \mathbf{N} \Sigma \mathbf{N} \boldsymbol{\mu}. \quad \blacksquare$$

We are now ready to state the proof of [Proposition 4.1](#):

*Proof.* This result follows directly from the expectation and variance of the quadratic functional, [Lemma B.1](#). For convenience, we express quantities with respect to the Euclidean inner product. By the scaling property of random normal vectors, we have  $\tilde{\mathbf{e}} := \mathbf{A} \mathbf{m} + \mathbf{B} \mathbf{z}^* + \mathbf{q} - \bar{\mathbf{u}} \sim \mathcal{N}(\mathbf{A} \mathbf{m}_{\text{MAP}}^y + \mathbf{B} \mathbf{z}^* + \mathbf{q} - \bar{\mathbf{u}}, \mathbf{A} \Gamma_{\text{post}} \mathbf{A}^* \mathbf{M}_u^{-1})$ , which lies in  $\mathbb{R}^n$ . Note that the covariance of  $\tilde{\mathbf{e}}$  is symmetric and positive-definite by construction. By [Lemma B.1](#) and the cyclic property of traces, we have

$$\begin{aligned} \mathbb{E}(\|\tilde{\mathbf{e}}\|_{\mathbf{M}_u}^2) &= \text{tr}[\mathbf{A} \Gamma_{\text{post}} \mathbf{A}^*] + \|\mathbf{A} \mathbf{m}_{\text{MAP}}^y + \mathbf{B} \mathbf{z}^* + \mathbf{q} - \bar{\mathbf{u}}\|_{\mathbf{M}_u}^2, \\ \text{Var}(\|\tilde{\mathbf{e}}\|_{\mathbf{M}_u}^2) &= 2 \text{tr}[(\mathbf{A} \Gamma_{\text{post}} \mathbf{A}^*)^2] + 4 \|\mathbf{A} \mathbf{m}_{\text{MAP}}^y + \mathbf{B} \mathbf{z}^* + \mathbf{q} - \bar{\mathbf{u}}\|_{\mathbf{M}_u \mathbf{A} \Gamma_{\text{post}} \mathbf{A}^*}^2 \end{aligned}$$

Scaling the random variable  $\|\tilde{\mathbf{e}}\|_{\mathbf{M}_u}^2$  by  $\frac{1}{2}$  gives the desired result. \blacksquare

**B.2. Hanson-Wright inequality and corollaries.** A useful tool for obtaining concentration bounds for sub-Gaussian random variables is the Hanson-Wright Inequality [31, 52]. We focus primarily on the application of this theorem to Gaussian random variables, which we state in [Theorem B.2](#).

**Theorem B.2 (Hanson-Wright Inequality: Special Case).** *Let  $\hat{\mathbf{z}} \sim \mathcal{N}(\mathbf{0}, \mathbf{I}_n)$  be a standard Gaussian random vector, and let  $\mathbf{N}$  be a symmetric matrix. Then, the quadratic random variable,  $Q(\hat{\mathbf{z}}) = \langle \hat{\mathbf{z}}, \mathbf{N}\hat{\mathbf{z}} \rangle$  satisfies,*

$$\mathbb{P}(|Q(\hat{\mathbf{z}}) - \mathbb{E}\{Q(\hat{\mathbf{z}})\}| \geq t) \leq 2 \exp \left[ -\frac{1}{8} \min \left\{ \frac{t}{\|\mathbf{N}\|_2}, \frac{t^2}{\|\mathbf{N}\|_F^2} \right\} \right]$$

for all  $t \geq 0$ .

*Proof.* From [20, Lemma 4]

$$\begin{aligned} \mathbb{P}(|Q(\hat{\mathbf{z}}) - \mathbb{E}\{Q(\hat{\mathbf{z}})\}| \geq t) &\leq 2 \exp \left[ -\frac{t^2}{4t\|\mathbf{N}\|_2 + 4\|\mathbf{N}\|_F^2} \right] \\ &\leq 2 \exp \left[ -\frac{t^2}{8 \max\{t\|\mathbf{N}\|_2, \|\mathbf{N}\|_F^2\}} \right]. \end{aligned}$$

The proof is completed by a simple manipulation of the upper bound. ■

**Remark B.3.** *Note that the constant  $1/8$  in Theorem B.2 can be replaced by any constant less than 0.14, as shown in [46, Lemma 1] and [47, Proposition 1]. The full proof of the Hanson-Wright inequality for sub-gaussian random variables can be referred to in [52]. An alternative proof pertaining to the special case of Gaussian random vectors can also be found in the proof of [24, Theorem B.8].*

**Theorem B.4 (Hanson-Wright Inequality: General Covariance).** *Let  $\mathbf{z} \sim \mathcal{N}(\mathbf{0}, \Sigma)$  be a Gaussian random vector where  $\Sigma \in \mathbb{R}^{n \times n}$  is a symmetric positive-definite covariance operator. Consider a matrix  $\mathbf{N} \neq \mathbf{0}$  and the induced quadratic random variable,  $Q(\mathbf{z}) = \langle \mathbf{z}, \mathbf{N}\mathbf{z} \rangle$ . Then,*

$$\mathbb{P}(|Q(\mathbf{z}) - \mathbb{E}\{Q(\mathbf{z})\}| \geq t) \leq 2 \exp \left[ -\frac{1}{8} \min \left\{ \frac{t}{\|\Sigma^{1/2}\mathbf{N}\Sigma^{1/2}\|_2}, \frac{t^2}{\|\Sigma^{1/2}\mathbf{N}\Sigma^{1/2}\|_F^2} \right\} \right]$$

for all  $t \geq 0$ .

*Proof.* Let  $\hat{\mathbf{z}} := \Sigma^{-1/2}\mathbf{z}$  and  $\hat{\mathbf{N}} := \Sigma^{1/2}\mathbf{N}\Sigma^{1/2}$ . Then,  $\langle \mathbf{z}, \mathbf{N}\mathbf{z} \rangle = \langle \hat{\mathbf{z}}, \hat{\mathbf{N}}\hat{\mathbf{z}} \rangle$ , so  $Q(\mathbf{z}) = \hat{Q}(\hat{\mathbf{z}})$ . Applying Theorem B.2 to the standardized random vector and the transformed matrix gives the desired result. ■

**Remark B.5.** *Note that in Theorem B.4, we can reformulate the norms to obtain a weaker but more comprehensible bound. In particular, note that by symmetry and cyclical commutativity of the trace,*

$$\|\Sigma^{1/2}\mathbf{N}\Sigma^{1/2}\|_F^2 = \text{tr} \left[ (\Sigma^{1/2}\mathbf{N}\Sigma^{1/2})^2 \right] = \text{tr} \left[ \Sigma^{1/2}\mathbf{N}\Sigma\mathbf{N}\Sigma^{1/2} \right] = \text{tr} \left[ (\Sigma\mathbf{N})^2 \right].$$

Since the two-norm is bounded above by the Frobenius norm, we have that

$$\|\Sigma^{1/2}\mathbf{N}\Sigma^{1/2}\|_2 \leq \|\Sigma^{1/2}\mathbf{N}\Sigma^{1/2}\|_F = \sqrt{\text{tr}[(\Sigma\mathbf{N})^2]}.$$

Inserting these bounds into the Hanson-Wright Inequality, we obtain the following alternative bound,

$$(B.6) \quad \mathbb{P}(|Q(\mathbf{z}) - \mathbb{E}\{Q(\mathbf{z})\}| \geq t) \leq 2 \exp \left[ -\frac{1}{8} \min \left\{ \frac{t}{\sqrt{\text{tr}[(\Sigma\mathbf{N})^2]}}, \frac{t^2}{\text{tr}[(\Sigma\mathbf{N})^2]} \right\} \right]$$

for all  $t \geq 0$ .

**Lemma B.6.** Consider  $Q(\mathbf{x})$  from (B.1). Then, for any  $t > 0$ ,  
(B.7)

$$\mathbb{P}(|Q(\mathbf{x}) - \mathbb{E}[Q(\mathbf{x})]| \geq t) \leq 4 \exp \left[ -\frac{1}{8} \min \left\{ \frac{t}{\sqrt{\text{tr}[(\mathbf{\Sigma}\mathbf{N})^2]}}, \frac{t^2}{\text{tr}[(\mathbf{\Sigma}\mathbf{N})^2]}, \frac{t^2}{(\mathbf{N}\boldsymbol{\mu})^\top \mathbf{\Sigma}(\mathbf{N}\boldsymbol{\mu})} \right\} \right].$$

*Proof.* Let  $\mathbf{z} := \mathbf{x} - \boldsymbol{\mu}$  be the centered random variable in  $\mathcal{N}(\mathbf{0}, \mathbf{\Sigma})$ . Then,

$$\begin{aligned} Q(\mathbf{x}) &= \langle \mathbf{x}, \mathbf{N}\mathbf{x} \rangle = \langle \mathbf{z} + \boldsymbol{\mu}, \mathbf{N}(\mathbf{z} + \boldsymbol{\mu}) \rangle \\ &= Q(\mathbf{z}) + 2\langle \mathbf{z}, \mathbf{N}\boldsymbol{\mu} \rangle + \langle \boldsymbol{\mu}, \mathbf{N}\boldsymbol{\mu} \rangle. \end{aligned}$$

By (B.6), note that for any  $t \geq 0$ ,

$$\mathbb{P}(|Q(\mathbf{z}) - \text{tr}(\mathbf{A}\mathbf{\Sigma})| \geq t) \leq 2 \exp \left[ -\frac{1}{8} \min \left\{ \frac{t}{\sqrt{\text{tr}[(\mathbf{\Sigma}\mathbf{N})^2]}}, \frac{t^2}{\text{tr}[(\mathbf{\Sigma}\mathbf{N})^2]} \right\} \right].$$

Moreover, note that  $\langle \mathbf{z}, \mathbf{N}\boldsymbol{\mu} \rangle$  is a Gaussian random variable with mean zero and variance  $(\mathbf{N}\boldsymbol{\mu})^\top \mathbf{\Sigma}(\mathbf{N}\boldsymbol{\mu})$ . Therefore, by a Chernoff bound [19], we have that

$$\mathbb{P}(|\langle \mathbf{z}, \mathbf{N}\boldsymbol{\mu} \rangle| \geq t) \leq 2 \exp \left[ -\frac{t^2}{2(\mathbf{N}\boldsymbol{\mu})^\top \mathbf{\Sigma}(\mathbf{N}\boldsymbol{\mu})} \right].$$

Using the triangle inequality and a union bound, we can combine the tail bounds to obtain that

$$\begin{aligned} \mathbb{P}(|Q(\mathbf{x}) - \mathbb{E}[Q(\mathbf{x})]| \geq t) &= \mathbb{P}(|Q(\mathbf{x}) - \text{tr}(\mathbf{N}) - \boldsymbol{\mu}^\top \mathbf{N}\boldsymbol{\mu}| \geq t) \\ &= \mathbb{P}(|Q(\mathbf{z}) + 2\langle \mathbf{z}, \mathbf{N}\boldsymbol{\mu} \rangle - \text{tr}(\mathbf{A})| \geq t) \\ &\leq \mathbb{P}(|Q(\mathbf{z}) - \text{tr}(\mathbf{N})| \geq t) + \mathbb{P}(|2\langle \mathbf{z}, \mathbf{N}\boldsymbol{\mu} \rangle| \geq t) \\ &\leq 2 \exp \left[ -\frac{1}{8} \min \left\{ \frac{t}{\sqrt{\text{tr}[(\mathbf{\Sigma}\mathbf{N})^2]}}, \frac{t^2}{\text{tr}[(\mathbf{\Sigma}\mathbf{N})^2]} \right\} \right] \\ &\quad + 2 \exp \left[ -\frac{t^2}{8(\mathbf{N}\boldsymbol{\mu})^\top \mathbf{\Sigma}(\mathbf{N}\boldsymbol{\mu})} \right]. \end{aligned}$$

We can combine the two exponential summands by their maximum, which provides the desired result. ■

**Proof of Proposition 4.2.** This result follows from the concentration bound for quadratic forms, Lemma B.6, which builds on the Hanson-Wright Inequality. As in the proof of Proposition 4.1, we consider  $\tilde{\mathbf{e}} := \mathbf{A}\mathbf{m} + \mathbf{B}\mathbf{z}^* + \mathbf{q} - \bar{\mathbf{u}} \sim \mathcal{N}(\mathbf{A}\mathbf{m}_{\text{MAP}} + \mathbf{B}\mathbf{z}^* + \mathbf{q} - \bar{\mathbf{u}}, \mathbf{A}\mathbf{\Gamma}_{\text{post}}\mathbf{A}^*\mathbf{M}_u^{-1})$  so that  $\Phi_{\text{ctrl}}^* = \|\tilde{\mathbf{e}}\|_{\mathbf{M}_u}^2$ . Since  $\mathbf{A}\mathbf{\Gamma}_{\text{post}}\mathbf{A}^*\mathbf{M}_u^{-1}$  is symmetric positive-definite, Lemma B.6 yields that for any  $t \geq 0$ , we have

$$\mathbb{P}(|\|\tilde{\mathbf{e}}\|_{\mathbf{M}_u}^2 - \mathbb{E}(\|\tilde{\mathbf{e}}\|_{\mathbf{M}_u}^2)| \geq \tau) \leq 4 \exp \left[ -\frac{1}{8} \min \left\{ \frac{\tau}{\sqrt{\text{tr}[(\mathbf{A}\mathbf{\Gamma}_{\text{post}}\mathbf{A}^*)^2]}}, \frac{\tau^2}{\text{tr}[(\mathbf{A}\mathbf{\Gamma}_{\text{post}}\mathbf{A}^*)^2]}, \frac{\tau^2}{C^2} \right\} \right],$$

where  $C$  is as defined in the statement. Recall that for a symmetric positive semi-definite matrix  $\mathbf{Z}$ ,  $\text{tr}[\mathbf{Z}^2] \leq \text{tr}[\mathbf{Z}]^2$ . Applying this result to  $\mathbf{Z} := \mathbf{M}_u^{1/2} \mathbf{A} \Gamma_{\text{post}} \mathbf{A}^* \mathbf{M}_u^{-1/2}$ , we have

$$(B.8) \quad \text{tr}[(\mathbf{M}_u^{1/2} \mathbf{A} \Gamma_{\text{post}} \mathbf{A}^* \mathbf{M}_u^{-1/2})^2] \leq [\text{tr}(\mathbf{M}_u^{1/2} \mathbf{A} \Gamma_{\text{post}} \mathbf{A}^* \mathbf{M}_u^{-1/2})]^2.$$

Notice that the trace is invariant under similarity transformation, i.e.,

$$\text{tr}(\mathbf{M}_u^{1/2} \mathbf{A} \Gamma_{\text{post}} \mathbf{A}^* \mathbf{M}_u^{-1/2}) = \text{tr}(\mathbf{A} \Gamma_{\text{post}} \mathbf{A}^*)$$

and

$$\text{tr}[(\mathbf{M}_u^{1/2} \mathbf{A} \Gamma_{\text{post}} \mathbf{A}^* \mathbf{M}_u^{-1/2})^2] = \text{tr}[\mathbf{M}_u^{1/2} (\mathbf{A} \Gamma_{\text{post}} \mathbf{A}^*)^2 \mathbf{M}_u^{-1/2}] = \text{tr}[(\mathbf{A} \Gamma_{\text{post}} \mathbf{A}^*)^2].$$

Thus, (B.8) simplifies to  $\text{tr}[(\mathbf{A} \Gamma_{\text{post}} \mathbf{A}^*)^2] \leq [\text{tr}(\mathbf{A} \Gamma_{\text{post}} \mathbf{A}^*)]^2$ . Substituting this inequality into the above probability bound achieves the desired result. ■

**Proof of Corollary 4.3.** The proof follows from a simple manipulation of the concentration bound (4.8). Namely, we want to obtain  $\tau$  such that the upper bound for the deviation probability in (4.8) is less than  $\delta$ , i.e., such that

$$4 \exp \left[ -\frac{1}{8} \min \left\{ \frac{\tau}{\Psi^{cA}}, \frac{\tau^2}{(\Psi^{cA})^2}, \frac{\tau^2}{C^2} \right\} \right] \leq \delta.$$

Rearranging and solving for  $\tau$  yields the upper bound in (4.9). ■